AD NUMBER
ADA145071

NEW LIMITATION CHANGE

TO

Approved for public release, distribution unlimited

FROM

Distribution authorized to DoD and DoD contractors only; Administrative/Operational use; Aug 1984. Other requests shall be referred to Air Force rocket Propulsion Lab, Edwards AFB CA. 93523

AUTHORITY

Per DoDD 5230.24, 18 Mar 1987

AFRPL TR-84-044

AD:

Final Report
for the period
1 March 1981 to
29 February 1984

HMX Combustion Modification

August 1984

Authors:
J. E. Flanagan
M. B. Frankel
D. O. Woolery

Rockwell International
Rocketdyne Division
6633 Canoga Avenue
Canoga Park, California 91304

F049626-81-C-0031
RI/RD84-144
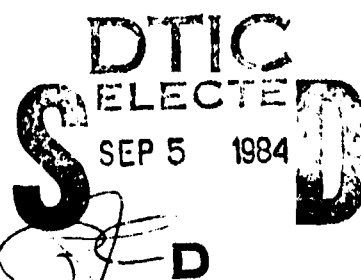
Subject to Export Control Laws

DTIC
ELECTE
SEP 5 1984
S
D

printed by the: **Air Force
Rocket Propulsion
Laboratory**

Air Force Space Technology Center
Space Division, Air Force Systems Command
Edwards Air Force Base,
California 93523

AD-A145 071

DTIC FILE COPY

84 08 31 028

NOTICES
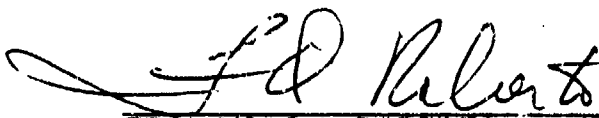
FOREWORD

MICHELE IRWIN
Project Manager

CHARLES W. BECKMAN
Chief, Formulation and Ingredient Section

FRANCISCO Q. ROBERTO
Chief, Propellant Development Branch

FOR THE DIRECTOR

HOMER M. PRESSLEY JR
Deputy Director, Solid Rocket Division

REPORT DOCUMENTATION PAGE

1a. REPORT SECURITY CLASSIFICATION		1b. RESTRICTIVE MARKINGS
Unclassified		

2a. SECURITY CLASSIFICATION AUTHORITY	3. DISTRIBUTION/AVAILABILITY OF REPORT
	Distribution limited to DoD agencies and
2b. DECLASSIFICATION/DOWNGRADING SCHEDULE	their contractors only; Critical Technology July 1984.

4. PERFORMING ORGANIZATION REPORT NUMBER(S)	5. MONITORING ORGANIZATION REPORT NUMBER(S)
RI/RD84-144	AFRPL-TR-84-044

6a. NAME OF PERFORMING ORGANIZATION	6b. OFFICE SYMBOL (If applicable)	7a. NAME OF MONITORING ORGANIZATION
Rockwell International Rocketdyne Division		Air Force Rocket Propulsion Laboratory

6c. ADDRESS (City, State and ZIP Code)	7b. ADDRESS (City, State and ZIP Code)
6633 Canoga Avenue Canoga Park, CA 91304	AFRPL/MKPA (Stop 24) Edwards AFB CA 93523

8a. NAME OF FUNDING/SPONSORING ORGANIZATION Air Force Office of Scientific Research	8b. OFFICE SYMBOL (If applicable)	9. PROCUREMENT INSTRUMENT IDENTIFICATION NUMBER
		F049626-81-C-0031

8c. ADDRESS (City, State and ZIP Code)	10. SOURCE OF FUNDING NOS.			
Air Force Office of Scientific Research Bolling AFB, Washington, D.C. 20332	PROGRAM ELEMENT NO.	PROJECT NO.	TASK NO.	WORK UNIT NO.

11. TITLE (Include Security Classification)
HMX Combustion Modification

12. PERSONAL AUTHOR(S)
J. E. Flanagan, M. B. Frankel, and D. O. Woolery

13a. TYPE OF REPORT	13b. TIME COVERED	14. DATE OF REPORT (Yr., Mo., Day)	15. PAGE COUNT
Final	FROM 81/03/01 TO 84/02/29	84/08	92

16. SUPPLEMENTARY NOTATION

17. COSATI CODES			18. SUBJECT TERMS (Continue on reverse if necessary and identify by block number)
FIELD	GROUP	SUB GR	HMX, RDX, Nitramines, Pyrolysis, Mass Spectrometry, Gas Chromatography, Burn Rates, Azides

19. ABSTRACT (Continue on reverse if necessary and identify by block number)

Studies were conducted during this 3-year program to gain a better understanding of the HMX decomposition mechanism by focusing upon the later stages of the multistep, complex decomposition process utilizing both isotopically labeled (N^{15}) and unlabeled HMX under low (~300 C) and high (~800 C) temperatures and at high heating rates. A novel experimental technique was developed, which utilized mass spectrometry and gas chromatography to identify quantitatively the amounts of gaseous species generated on pyrolysis of the substrates. This permitted detection of any chemical and/or thermal interactions between various energetic materials and an understanding of those interactions that contributed or deterred the burn rate of HMX or RDX.

20. DISTRIBUTION/AVAILABILITY OF ABSTRACT	21. ABSTRACT SECURITY CLASSIFICATION
UNCLASSIFIED/UNLIMITED ☒ SAME AS RPT ☒ DTIC USERS ☐	Unclassified

22a. NAME OF RESPONSIBLE INDIVIDUAL	22b. TELEPHONE NUMBER (Include Area Code)	22c. OFFICE SYMBOL
J. E. Flanagan	(818) 710-2466	

DD FORM 1473, 83 APR EDITION OF 1 JAN 73 IS OBSOLETE.

3. Distribution limited to DoD agencies and their contractors only; Critical
    Technology, April 1984. Other requestors for this document must be
    referred to AFRPL/TSTR (Stop 24) Edwards AFB, CA 93523.

19. Compounds that yielded NH_3^n, were oxygen free, and decomposed exothermi-
    cally, were demonstrated to have a significant effect upon the decompo-
    sition of HMX via an exothermic gas-phase reduction of NO (a decomposi-
    tion product of HMX). This effect was caused by the formation of
    amidogen (NH_2^n) radicals from the generated NH_3^n.

    Pyrolysis studies performed on various azide compounds showed that the
    azide moiety increased the burn rate of HMX primarily by a thermal
    effect due to the decomposing azide functionality.

    It also was shown that a close matching of the decomposition temperatures
    of HMX and the additive was required to enhance the chemical and/or
    thermal interactions between the gaseous decomposition products.

    Attempts to incorporate the azide group into the HMX structure were
    successful. By means of a multistep synthesis sequence, the compound
    1-azidomethyl-3,5,7-trinitro-1,3,5,7-tetrazacyclooctane was prepared.
    Pyrolysis of this compound, however, demonstrated that the mode of its
    decomposition was altered significantly from that of HMX. Its incor-
    poration in propellants containing HMX did not result in an enhanced
    burn rate.

Accession For

NTIS GRA&I	☐
DTIC TAB	☒
Unannounced	☐
Justification	

By

Distribution/

Availability Codes

Dist	Avail and/or Special
C/2	

CONTENTS

ILLUSTRATIONS

TABLES

ACKNOWLEDGEMENTS

SUMMARY

HMX decomposition studies performed under this contract have focused on the covalent bond-breaking processes occurring in the later stages of HMX decomposition in the liquid and gas phases. Emphasis was placed on a quantitative determination of gas-phase species from HMX decomposition using isotopically labeled (N^{15}) and unlabeled materials at high heating rates (850 C per second) under a helium atmosphere. Changes in the gas-phase product distributions from HMX decompostion in a low (~300 C) and high (~800 C) temperature region led to an understanding of the changing and competitive covalent bond-breaking processes occurring as the decomposition temperature increased. In addition, the detailed study of the interactive chemistry between energetic additives with HMX and correlation with propellant burn rate data has resulted in a better understanding of those processes that lead to an increased burn rate.

The thermal decomposition of HMX in the low-temperature region just above its liquefaction region (~300 C) proceeds primarily by C-N bond breaking, which results in high N_2O and CH_2O yields. In the high-temperature region (~800 C), N-N bond scission is faster than C-N bond breaking, and NO is formed in high yields. Gas-phase reduction of NO by NH_2 intermediates appears to play a key role in modifying HMX combustion. Tracer studies performed with ring N^{15} labeled material have shown that the NO is reduced to N_2 and H_2O by NH_3 generated from the decomposition of bistriamino-guanidinium azobitetrazole (TAGZT).

Compounds that are high in NH_3 or TAG content do not yield high concentrations of NH_3 decomposition products unless they are oxygen free. Also, compounds that appear to explode upon decomposition (such as DAZT) are not effective NH_3 generators despite their high initial NH_3 content.

Propellants containing TAGZT and the energetic plasticizer TMETN ($-ONO_2$) yielded the same relative increase in burning rate (~150%) as those that included the inert (triacetin) plasticizer. These results indicate that the NH_3 decomposition products are interacting primarily with the HMX products rather than the binder components.

1

Additional NH_3 generators were studied via high-temperature pyrolysis and burning rate experiments. The concentration of the NH_3 generated, the temperature of generation, and the physical process of generation were found to be the key factors in the overall effectiveness in accelerating the burning rate.

A critical parameter, the relative particle size of the nitramine to the NH_3 generating compound, was defined, which is related to the diffusional flame characteristics. The efficiency of the NH_2 + NO reaction optimizes over a narrow temperature region ($\sim$1100 $\rightarrow$ 1300 K) and the reaction is very sensitive to the concentration of a variety of active species.

Substitution and coprecipitation of azide nitramines (such as DATH) definitely accelerate the burning rate, but it appears to be via an "additive" mechanism rather than an interaction process.

The energetic compound triaminoguanidinium-5-aminotetrazole (TAG·5AT) was observed to generate high yields of NH_3 on decomposition at 800 C. However, this compound was shown to burn at ambient pressure with liquefaction and an overall cooling effect, which is probably due to the excess NH_3 generated. Pyrolysis decomposition studies of HMX in the presence of TAG·5AT at 800 C indicated a reduced degree of NO reduction by NH_2 intermediates as compared to TAGZT. In addition, an increase in N_2O yield from HMX-TAG·5AT decomposition is indicative of a contributing "cooling" affect from TAG·5AT. As expected, smaller changes in HMX-TAG·5AT propellant burn rate were encountered.

From pyrolysis decomposition studies, it has been shown that the well-known energetic compound triaminoguanidine nitrate (TAGN) undergoes exothermic NO reduction to N_2 by NH_2 intermediates generated from TAGN itself. Thus, the reported increase in HMX burn rate by the addition of TAGN is due primarily to an "additive" effect. A secondary process of NO reduction in the TAGN system is controlled by diffusional flame phenomena, which is coupled via particle-size ratios.

Pyrolysis decomposition studies performed on 98 weight percent HMX admixed with 2 weight percent LiN_3 or NaN_3 at 800 C showed a dramatic change in the HMX decomposition mechanism. Although both LiN_3 and NaN_3 appear to display a catalytic effect in altering the HMX decomposition mechanism, significant changes in HMX propellant burn rates were not encountered. Intimate contact is believed to be lost between the active catalyst intermediates LiN_3 or NaN_3 in propellant mixes.

The thermal decomposition of RDX proceeds in an identical fashion as HMX at ~800 C with $N-NO_2$ bond scission being faster than C-N bond scission, which results in high NO yields. However, in the temperature region just above the liquefaction of RDX (~220 C), gas phase product distributions from RDX indicate a faster rate of RDX liquefaction to gasification. RDX undergoes 90% pyrolysis (with comparable C-N and $N-NO_2$ bond scission) just above the liquefaction region versus only 70% pyrolysis for HMX (with predominant C-N bond scission).

The Werner-diammoniumdiazido complex $[Cu(NH_3)_2(N_3)_2]$, which generates significant NH_3 on decomposition, was shown to significantly alter the decomposition mechanism of RDX at the 5 weight percent level, but had little influence on the HMX decomposition mechanism. $[Cu(NH_3)_2(N_3)_2]$ undergoes violent decomposition at 210 C, which is much closer to the RDX decomposition temperature of 201 C, allowing for a greater thermal and/or chemical interaction than that of HMX undergoing decomposition at 280 C.

Synthesis of the novel HMX derivative 1-azidomethyl-3,5,7-trinitro-1,3,5,7-tetrazacyclooctane (AZMTTC) is reported. Pyrolysis decomposition studies conducted on AZMTTC showed that its decomposition mechanism is significantly different from that of HMX. Carbon-nitrogen bond scission predominates during the decomposition of AZMTTC from ~300 to ~800 C, which results in high N_2O and CH_2O yields. This mode of decomposition is not conducive to increasing burn rates as a result of reduced bond scission and the nature of the gas-phase components generated. It is believed that structural symmetry of the HMX derivative must be maintained to arrive at comparable rates of C-N and $N-NO_2$ bond scission along with gas-phase components, which will generate increased exothermic gas-phase reactions.

3

The unsuccessful attempts at the synthesis of a structurally symmetrical HMX derivative from the recently reported HMX precursor DADN are reported. In addition, attempts to synthesize other unsymmetrical HMX derivatives via novel synthetic procedures used in the synthesis of AZMTTC are described.

The burning rate acceleration of HMX-based propellants was achieved most readily with amidogen radical generators, especially TAGZT. The magnitude of augmentation of the HMX propellants is virtually the same regardless of the type of plasticizer employed, except for the NF type (TVOPA). This suggests a higher rate of interaction between the NH_2 and NF_2 radicals in a "pseudocatalytic" manner.

The burning rate acceleration of RDX-based propellants followed similar trends to the HMX systems except at low pressures (<3.45 MPa). In the low-pressure region, the RDX systems burned 20 to 80% faster than the HMX analog. This is attributed to the fact that the NH radical generating ingredients decompose at a temperature closer to the decomposition point of RDX rather than HMX, thereby promoting a higher level of interaction. As the pressure is increased, the diffusional flame is compressed and similar acceleration would be expected.

The "mismatching" of the nitramine (HMX and RDX) and amidogen generator particle sizes appears to be the most important factor in accelerating the rate. Utilization of small additive particle sizes with large nitramine particles results in better diffusional mixing of the reactive gases.

4

SECTION 1

OBJECTIVE

The objective of this research program was to increase the burning rate of
cyclic nitramines (HMX and RDX) via (1) chemical doping, (2) structural modi-
fication, and (3) the addition of modifiers that generated reactive inter-
mediates. Primary emphasis was placed on the incorporation of azido ($-N_3$)
moieties and addition of ingredients for amidogen ($-NH_2$) radical genera-
tion. Pyrolysis studies were conducted at rapid heating rates with and
without isotopically (N^{15}) labeled materials as the primary screening tool
for measuring the effectiveness of these approaches and guiding the
formulation of experimental propellants.

SECTION 2

INTRODUCTION

The utilization of HMX and RDX in solid and gun propellant applications is increasing rapidly. In the solid propellant arena, the desire for reduced smoke (signature) has eliminated ammonium perchlorate (AP) from consideration in a wide variety of applications. For gun propellants, the desire for increased mass impetus at reduced flame temperatures has resulted in the blending of HMX and RDX with selected high-hydrogen content oxidizers such as triaminoguanidine nitrate (TAGN) in extruded nitrocellulose binder systems.

However, both HMX and RDX have low burning rates at low pressures (<14 MPa). This is coupled with high exponent problems, especially in the gun propellant area, for pressures up to 425 MPa. The gun propellant problem can be alleviated to a great degree by proper selection of alternate secondary oxidizers, grinding of the nitramine to small particle size (>5μ), and through judicious grain design. This freedom is not totally available to the solid propellant designer since his systems require excellent physical properties and must be cast instead of solvent extruded. It is imperative that methods for accelerating the burning rate of HMX and RDX and controlling the exponent be developed to ensure the solid propellant grain designer adequate freedom in meeting advanced applications while maintaining the energy level of the system.

The aforementioned objectives of this research program were deemed to be a unique approach to delineating the problems faced by the propellant community.

DECOMPOSITION EXPERIMENTS

HMX DECOMPOSITION MECHANISMS -- AN OVERVIEW

There is voluminous literature on studies of the thermal decomposition of HMX
with evidence to support the cleavage of every covalent bond including the
C-N bond, the N--NO$_2$ bond, tne N--O bond, and the C-H bond, with conclusions
suggesting each of these as a likely initial and/or rate-controlling intra-
molecular process. Recently, evidence has been given to support the conclu-
sions that the electrostatic intermolecular attractions between structurally
intact HMX molecules is the initial rate-controlling process and predom-
inantly controls the rate of solid and liquid HMX decomposition (Ref. 1).
This novel conclusion contrasts with all previous interpretations of
condensed-phase HMX decomposition kinetics, which assumed that intramolecular
covalent bond breaking within the HMX molecule controls the decomposition
kinetics. However, these investigators also concluded that the covalent
bond-breaking processes described by others were occurring likely in the same
time frame as the breakdown of intermolecular electrostatic forces, but they
were not necessarily rate determining.

Other recent studies, using deuterium isotope effects with HMX, have shown
C-H covalent bond cleavage to be a rate-controlling intramolecular process in
the solid phase, but C-H bond contraction occurring in a mixed solid-liquid
phase (Ref. 2).

The presence of NO$_2$ radical species in solid-phase HMX has been demon--
strated recently by mechanical methods or irradiation and contributes to the
list of potentially reactive species in the early stages of HMX decomposition
(Ref. 3).

Many HMX decomposition mechanisms have been inferred from gas-phase species
that could have originated in a combination of solid, liquid, and gas phases
of HMX decomposition with the false assumption that the analysis is conducted
in one phase. The simultaneous occurrence of these various intermolecular
and intramolecular processes in the solid, liquid, and gas phase within a

relatively short time frame enables one to appreciate the unique and vastly complex nature of HMX decomposition (an overall decomposition schematic is given in Table 1). In addition, an understanding of these processes allows one to realize the experimental difficulty in obtaining a homogeneous or reproducible HMX sample during thermal decomposition studies. Thus, the chemistry associated with HMX decomposition is occurring in a neterogeneous system and care must be taken to adequately describe experimental procedures and sampling techniques. Furthermore, conclusions that isolate one molecular process as controlling the multistep complex HMX decomposition mechanism that involves a number of molecular processes occurring almost simultaneously must be avoided.

EXPERIMENTAL DETAILS

Product distributions from the thermal decomposition of unlabeled, ring N^{15} labeled and total N^{15} labeled HMX, and candidate additives for modifying the decomposition characteristics of HMX were investigated using a Chemical Data Systems Series 100 pyrolysis unit interfaced with a Hewlett-Packard 5840A gas chromatograph and Inficon 1Q200 quadrupole mass spectrometer (Fig. 1). Samples (0.5 to 1.5 milligrams) of these materials were weighed accurately within a thin-walled quartz tube, which was placed within a platinum coil pyrolysis probe and inserted into a heated gas chromotographic interface under 2 atm helium back pressure. The samples were pyrolyzed at a maximum heating rate of approximately 850 C per second and held for 10 seconds at temperature in all experiments. Upon pyrolysis, the gaseous products (H_2, N_2, NO, CO, N_2H_4, CH_4, H_2O, NH_3, CO_2, N_2O, CH_2O, HCN, and $CH_2 = CH_2$) were separated in the order given on a 6-foot by 0.125-inch stainless-steel column packed with Carbosieve S, 120-140 mesh (Supelco Inc.). Other pertinent gas chromatographic operating procedures are given in Table 2. The experimental setup also allowed for injection of the separated gaseous species into the mass spectrometer for a determination of the mass fragmentation patterns of the labeled and unlabeled gas-phase species. Quantitative calibrations were performed on control samples of all gases, and their identification was confirmed by introduction of the gases into the mass spectrometer. All tabulated data are the result of replicate experiments conducted under identical experimental conditions.

TABLE 1. HMX DECOMPOSITION - AN OVERVIEW

TEMPERATURE, C	PHYSICAL STATE	MOLECULAR PROCESSES INFLUENCING HMX DECOMPOSITION	RESULT
<160	SOLID	A. STRONG ELECTROSTATIC INTERACTIONS B. CRYSTAL LATTICE IMPERFECTIONS	A. β-CRYSTAL CONFORMATION B. NO_2 RADICALS DETECTED
160-260	SOLID	A. ELECTROSTATIC INTERACTIONS WEAKENING B. CRYSTAL LATTICE IMPERFECTIONS C. C-H COVALENT BOND WEAKENING D. C-N COVALENT BOND WEAKENING	A. Δ-α-γ CRYSTAL CONFORMATIONS B. NO_2 RADICALS INCREASING C. HYDROGEN ATOM GENERATION D. RING CLEAVAGE
260-280	SOLID-LIQUID	A. ELECTROSTATIC INTERACTIONS VERY WEAK B. C-H COVALENT BOND CLEAVAGE C. C-N COVALENT BOND CLEAVAGE D. N-NO_2 COVALENT BOND CLEAVAGE	A. CRYSTAL CONFORMATIONS ABSENT B. HYDROGEN ATOM GENERATION C. N_2O AND CH_2O GENERATION D. NO_2 GENERATION
280-300	LIQUID-GAS	A. C-N COVALENT BOND CLEAVAGE B. N-NO_2 COVALENT BOND CLEAVAGE C. C-H COVALENT BOND CLEAVAGE D. EXOTHERMIC CH_2O + NO_2 REACTION	A. N_2O AND CH_2O GENERATION B. NO_2 GENERATION C. HYDROGEN ATOM GENERATION D. NO, CO, H_2O GENERATION
>300	GAS	A. SECONDARY LIQUID-GAS, GAS-GAS REACTIONS	A. NO, N_2O, N_2, HCN, CO, CO_2, CH_4, H_2, H_2O GENERATION

```
┌──────────┐     ┌──────────────┐     ┌──────────────┐     ┌──────────┐
│ PYROLYSIS│─────┤     GAS      │─────┤     MASS     │─────┤  VIDEO   │
│   UNIT   │─────┤ CHROMATOGRAPH│─────┤ SPECTROMETER │─────┤  COPIER  │
└──────────┘     └──────────────┘     └──────────────┘     └──────────┘
     I                 II                   III                 IV
```
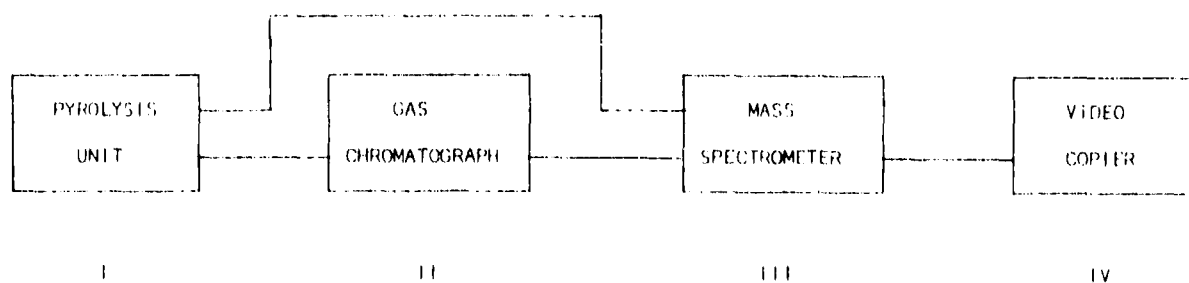
I.   CHEMICAL DATA SYSTEMS SERIES 100 PYROLYSIS UNIT WITH EXTENDED PROGRAM

II. HEWLETT PACKARD MODEL 5840A GAS CHROMATOGRAPH WITH THERMAL CONDUCTIVITY DETECTOR

III. INFICON IQ200 QUADRUPOLE MASS SPECTROMETER

IV. INFICON IMC-2 MEMORY COPIER

Figure 1.   Experimental Apparatus for Pyrolysis Studies

**TABLE 2.   GAS CHROMATOGRAPHIC OPERATING CONDITIONS FOR
SEPARATION OF GAS-PHASE DECOMPOSITION PRODUCTS**

COLUMN	6-FOOT BY 0.125-INCH STAINLESS-STEEL PACKED WITH CARBOSIEVE S, 120-MESH (SUPELCO INC.)
PYROLYSIS INTERFACE TEMPERATURE	140 C
TEMPERATURE PROGRAM	ISOTHERMAL 35 C FOR 4 MINUTES; THEN 20 C PER MINUTES TO 175 C FOR 20 MINUTES
THERMAL CONDUCTIVITY DETECTOR TEMPERATURE	260 C
ATTENUATION	6
HELIUM FLOW	50 MILLILITERS PER MINUTE

Vacuum pyrolysis experiments were carried out on unlabeled and N^{15} labeled (ring and total nitrogen) HMX. The samples were pyrolyzed under 0.03 mm vacuum and the decomposition products injected directly into the mass spectrometer through a molecular leak into the ionizing chamber with all surfaces preheated to 140 C. Mass fragmentation patterns and relative intensities for all m/e values were recorded then. In the quadrupole mass spectrometer, the pyrolysis products are bombarded by a current of 70 eV electrons giving rise to positively charged ions. A spectrum is produced by sweeping the quadrupole filter over the desired m/e range (0 to 200).

HMX (Ring N^{15} Labeled) Decomposition

Samples of ring N^{15} labeled HMX were pyrolyzed just above its melt region (~300 C) under 2 atm of helium. Under these conditions, the predominant gaseous product formed in the early stages of HMX decomposition was nitrous oxide (N_2O) in an amount equivalent to 51 mole percent (m/o) of the total HMX nitrogen. The identity and amounts of the other pyrolysis gases formed are summarized in Table 3. These conditions resulted in the pyrolysis of approximately 70 w/o of the samples.

Mass spectrometric analyses of the separated product gases provided information relative to the isotopic labeling of the nitrogen-containing products (Table 4). These results clearly demonstrated the two principal nitrogen species, N_2O and N_2, to be predominantly $N^{15}N^{14}O$ and $N^{15}N^{14}$. Thus, formation of N_2O and N_2 does not involve N-NO_2 bond cleavage under these conditions.

The third nitrogen-containing gaseous product, NO, was principally $N^{14}O$, which suggests that it was derived primarily from the -NO_2 group. Hydrogen cyanide, HCN, was not formed under these conditions, which implies a rate-controlling process (Ref. 4).

PRODUCT	WEIGHT PERCENT YIELD	MOLE PERCENT YIELD FROM N	MOLE PERCENT YIELD FROM C
N_2	10	26	
NO	15	18	
N_2O	31	51	
NH_3	1	2	
HCN	0	0	0
CO	5		13
CO_2	11		19
CH_2O	11		26
CH_4	1		5
H_2	0		
H_2O	9		
	94	97	65

*SAMPLE WAS 70% PYROLYZED.

TABLE 4. LABELED GASEOUS PRODUCT DISTRIBUTION FOR HMX
(RING N^{15}) PYROLYSIS (~300 C, 10 SECONDS, 2 ATM HELIUM*)

LABELED PRODUCT	MASS NO.	RELATIVE PERCENT INTENSITY	MOLE PERCENT CONTRIBUTION FROM TOTAL N	MOLE PERCENT YIELD BASED ON TOTAL N
$N^{14}N^{14}$	28	0	0	
$N^{15}N^{14}$	29	95	25	26
$N^{15}N^{15}$	30	5	1	
$N^{14}=O$	30	90	16	
$N^{15}=O$	31	10	2	18
$N^{14}=N^{14}=O$	44	0	0	
$N^{15}=N^{14}=O$	45	98	50	51
$N^{15}=N^{15}=O$	46	2		
HC N^{14}	27	0	0	
HC N^{15}	28	0	0	0

*SAMPLE WAS 70% PYROLYZED

Samples of the ring N^{15} labeled HMX also were pyrolyzed at high temperature (~800 C) under 2 atm of helium. Under these conditions, NO was the principal gaseous product and accounted for 42 m/o of the total HMX nitrogen (Table 5). The other two major nitrogen-containing gaseous products were N_2 (21 m/o) and N_2O (18 m/o). The pyrolysis of HMX at 800 C was near quantitative.

TABLE 5. GASEOUS PRODUCT DISTRIBUTION FROM HMX (RING N^{15})
PYROLYSIS (~800 C, 10 SECONDS, 2 ATM HELIUM)

PRODUCT	WEIGHT PERCENT YIELD	MOLE PERCENT YIELD FROM N	MOLE PERCENT YIELD FROM C
N_2	8	21	
NO	35	42	
N_2O	11	18	
NH_3	0	0	
HCN	13	17	35
CO	12		32
CO_2	11		19
CH_2O	0		0
CH_4	<1		<5
H_2	<1		
H_2O	10		
	100	98	36

Based on the results summarized in Tables 3 and 5, the major differences observed for the amounts of the nitrogen-containing product gases formed at ~300 versus ~800 C were as follows:

1. The formation of N_2O decreased significantly at the higher temperature

2. The amount of NO formed at ~800 C was greater

3. A slight decrease was observed in the N_2 yield

4. A significant amount of HCN was formed at the higher temperature

5. No NH_3 was observed at the higher pyrolysis temperature

A similar comparison of the carbon-containing product gases indicates the following with increased temperature:

1. An increase in the amount of CO

2. A decrease in the yield of CH_2O from 28 to 0 m/o

3. Virtually no change in the amounts of CO_2 and CH_4

Mass spectrometric analyses of the product gases obtained at ~800 C are summarized in Table 6. The isotopic compositions of N_2O and NO were predominantly $N^{15}N^{14}O$ and $N^{14}O$, as was observed for the pyrolysis of HMX at the lower temperature. The isotopic composition of the N_2 gas was somewhat different than previously observed in that the amounts of $N^{14}N^{14}$ and $N^{15}N^{15}$ were higher. The major amount of HCN was comprised of N^{15}, which supports the conclusion that it was formed from ring labeled N^{15}.

TABLE 6. LABELED GASEOUS PRODUCT DISTRIBUTION FROM HMX
(RING N^{15}) PYROLYSIS (~800 C, 10 SECONDS, 2 ATM HELIUM)

LABELED PRODUCT	MASS NO.	RELATIVE PERCENT INTENSITY	MOLE PERCENT CONTRIBUTION FROM TOTAL N	MOLE PERCENT YIELD BASED ON TOTAL N
$N^{14} \equiv N^{14}$	28	15	3	
$N^{15} \equiv N^{14}$	29	75	16	21
$N^{15} \equiv N^{15}$	30	10	2	
$N^{14} = O$	30	90	38	
$N^{15} = O$	31	10	4	42
$N^{14} = N^{14} = O$	44	0	0	
$N^{15} = N^{14} = O$	45	95	17	18
$N^{15} = N^{15} = O$	46	5	1	
$HC \equiv N^{14}$	27	15	2	
$HC \equiv N^{15}$	28	85	15	17

Secondary N$_2$O Gas-Phase Reaction Considerations

Explanations were sought for the observed differences in the N$_2$O and NO yields as a function of increasing temperature. The observed increased NO yield, for example, might be due to secondary gas-phase reactions of N$_2$O. A possible N$_2$O gas-phase reaction is (Ref. 5):

$$N_2O + O \rightarrow 2NO \qquad\qquad E_a = 24 \text{ kcal/mole}$$

This should give equal parts of $N^{14}O$ and $N^{15}O$ from the observed $N^{15}N^{14}O$. However, since 90% of the recovered NO at high temperature was $N^{14}O$, this reaction does not appear to be a predominant one. A more likely explanation for the higher yield of NO is based on the previously reported work of Axworthy et al. (Ref. 4), who showed that NO was formed predominantly from HMX primary pyrolysis processes and not by secondary gas-phase reactions.

Nitrous oxide also is known to undergo the following reactions leading to N$_2$ formation (Ref. 5).

$$N_2O + O \rightarrow N_2 + O_2 \qquad\qquad E_a = 0.5 \text{ kcal/mole}$$

$$N_2C + CO \rightarrow N_2 + CO_2 \qquad\qquad E_a = 17 \text{ kcal/mole}$$

$$N_2O + M \rightarrow N_2 + O + M \qquad\qquad E_a = 51 \text{ kcal/mole}$$
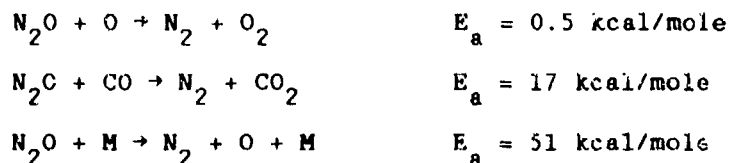
(where M is an inert species)

These reactions would give $N^{15}N^{14}$ from $N^{15}N^{14}C$. Thus, the observed $N^{15}N^{14}$ may have resulted from secondary N$_2$O reactions. However, since the N$_2$ yield decreased only slightly with increasing temperature, the large N$_2$O decrease cannot be accounted for totally by such secondary reactions. Finally, reactions of N$_2$O with carbon species that might result in the formation of HCN are unlikely.

The observed experimental results for the NO and N_2O yields versus pyrolysis temperature are in agreement with the work of Axworthy (Ref. 4). The conclusions are that the yields are the result of primary pyrolysis processes and not secondary gas-phase reactions. In separate experiments performed on the pyrolysis of RDX, it was found that the yields of N_2O and CH_2O were only half those from HMX and that the NO yields were greater at temperatures below 800 C.

Since the N_2O and NO yields are due to primary pyrolysis processes, the larger N_2O and CH_2O yields from HMX imply a weaker C-N bond strength (greater ring strain) than that of RDX. This is in agreement with the calculated thermodynamic estimates made by Shaw and Walter (Ref. 6). Thus, from the data obtained here and those previously mentioned, C-N bond breaking in HMX occurs to a greater extent than $N-NO_2$ bond cleavage near the melt region. As the temperature is increased, the $N-NO_2$ bond scission proceeds at a faster rate than C-N bond rupture, which results in greater NO yields.

Although the current work indicates that N_2O and N_2 form without rupture of the $N-NO_2$ bond, the conclusion that the initiation step cannot involve cleavage of the $N-NO_2$ bond is unwarranted. This would be true only if all of the nitrogen atoms in the parent HMX molecule ended up as N_2O and N_2. Based on the experimental results, this is not the case since 18 m/o NO was recovered just above the melt region of HMX. Therefore, the initial step could be a rupture of the $N-NO_2$ bond leading to nitrogen dioxide (NO_2) or nitrous acid (HONO) elimination followed by NO formation from these unstable species.

Vacuum Decomposition of Isotopically Labeled and Unlabeled HMX

The decomposition mechanism of N^{15} labeled and unlabeled HMX was investigated further at ~800 C (10 seconds) under vacuum (0.03 mm) The pyrolysis gases were injected directly into the mass spectrometer to determine all gaseous species initially formed. The resulting mass fragmentation patterns were quite complex (Tables 7 through 9). Therefore, a theoretical analysis

TABLE 7. MASS FRAGMENTATION PATTERN FOR GASEOUS PRODUCTS FROM HMX PYROLYSIS (~800 C, 10 SECONDS, 0.03 mm)

m/e	POSSIBLE SPECIES	RELATIVE INTENSITY (THEORETICAL)	
1	H	25	
2	H_2	33	
12	C	7	(6)
13	CH	3	(1)
14	N, CH_2	18	(15)
15	NH, CH_3	19	(3)
16	O, NH_2	15	(9)
17	OH, NH_3	40	(9)
18	H_2O	70	(36)
19	H_3O^+	1	(0.3)
22	CO_2^{++}	1	(0)
26	CN	6	(6)
27	HCN	22	(39)
28	CO, N_2, CH_2N	30	(72)
29	CH_2NH, CH_3N, CHO	24	(0.3)
30	NO, CH_2O	100	(100)
31	CH_5O, HNO	4	(3)
39	CNCH	1	(0)
40	CNN, $CNCH_2$, NCN	1	(0)
41	NCHN, HCNCH	1	(0)
42	N_2O, H_2CNN, CH_2NC, NCH_2N	4	(0)
43	HOCN, NCH_2N	26	(0)
44	N_2O, CO_2, CH_2NO	100	(60)
45	HNNO	4	(0.3)
46	NO_2	2	(0)

17

TABLE 8. MASS FRAGMENTATION PATTERN FOR GASEOUS PRODUCTS FROM HMX (RING N^{15}) PYROLYSIS (~800 C, 10 SECONDS, 0.03 mm)

m/e	POSSIBLE SPECIES	RELATIVE INTENSITY
1	H	18
2	H_2	25
12	C	4
13	CH	1
14	N, CH_2	8
15	N^{15}, CH_3, NH	3
16	O, $N^{15}H$	10
17	OH, $N^{15}H_2$, NH_3	23
18	H_2O, $N^{15}H_3$	65
19	H_3O^+	1
22	CO_2^{++}	1
26	CN	2
27	CN^{15}, HCN	6
28	CO, HCN^{15}, CH_2N, N_2	46
29	$N^{15}N^{14}$, CH_2N^{15}, CH_2NH, CH_3N, CHO	18
30	NO, CH_2O, N_2^{15}, $CH_2N^{15}H$, CH_3N^{15}	100
31	CH_3O, $N^{15}O$, HNO	4
39	CNCH	1
40	CNN, $CNCH_2$, $CH^{15}CH$, CHNCH	1
41	NCHN, $HCNCH_2$, $CH^{15}N^{14}$, $CN^{15}CH_2$	1
42	H_2CNN, CH_2NCH_2, $CH^{15}N^{15}$, $N^{15}CHN$, $HCN^{15}CH_2$, OCN	2
43	$CH_2N^{15}CH_2$, HOCN, $H_2CN^{15}N$, $N^{15}CHN^{15}$, OCN^{15}	3
44	CO_2, N_2O, $HOCN^{15}$, $N^{15}CH_2N^{15}$, CH_2NO, $N^{15}CH_2NH$	55
45	$N^{15}N^{14}O$, $N^{15}CH_2N^{15}H$, ENNC	22
45	NO_2, $HN^{15}NO$	1

TABLE 9. MASS FRAGMENTATION PATTERN FOR GASEOUS PRODUCTS FROM HMX (TOTAL N^{15}) PYROLYSIS (~800 C, 10 SECONDS, 0.03 mm)

m/e	POSSIBLE SPECIES	RELATIVE INTENSITY
1	H	20
2	H_2	24
12	C	6
13	CH	1
14	CH_2	4
15	N^{15}, CH_3	11
16	O, $N^{15}H$	12
17	OH, $N^{15}H_2$	34
18	H_2O, $N^{15}H_3$	85
19	H_3O^+	1
22	CO_2^{++}	1
27	CN^{15}	9
28	CO, HCN^{15}	45
29	CH_2N^{15}, CHO	23
30	$N^{15}N^{15}$, $CH_2N^{15}H$, CH_3N^{15}, CH_2O	42
31	$N^{15}O$, CH_3O	1?0
40	$CN^{15}CH$	?
41	$CN^{15}CH_2$, $CHN^{15}CH$	1
42	$CN^{15}N^{15}$, $HCN^{15}CH_2$	?
43	$CH_2N^{15}CH_2$, OCN^{15}	4
44	CO_2, $HOCN^{15}$, $H_2CN^{15}N^{15}$	58
45	$N^{15}CH_2N^{15}H$, $CH_2N^{15}O$	2
46	$N^{15}N^{15}O$	30
47	$N^{15}O_2$, $HN^{15}N^{15}O$	?

of the mass fragmentation patterns was performed. The basis for the analysis was the mass spectral data reported by Cornu (Ref. 7) for those gaseous products found during the HMX pyrolysis studies conducted at ~800 C under 2 atm of helium. Table 10 is a compilation of Cornu's mass spectral data, and the relative intensities given are based on the reference gas n-butane.

The data summarized in Table 10 indicate the complex mass fragmentation pattern one might expect based on the listed gases. The w/o product gas yields from the pyrolysis of HMX at ~800 C in 2 atm of helium are summarized in Table 11. Based on the assumption that the product gas yields are similar at 800 C under 2 atm of helium or 0.03 mm of pressure, one can predict a theoretical mass fragmentation pattern for the product gases due to electron bombardment. This theoretical fragmentation pattern is given at the bottom of Table 10 for which a mass of 30 (NO) was used as a baseline with a relative intensity of 100. The following discussion will refer to this theoretical fragmentation pattern for which there are significant differences.

The m/e values of 1 and 2 (Table 7) are due to H atoms and H_2, respectively. As shown in Table 11, the H_2 yields were less than 1 w/o.

The m/e value of 15 (Table 7) is several times larger than that predicted (Table 10), which suggests that NH or CH_3 formation from HMX results from primary and/or secondary thermal decomposition processes, and is not totally due to mass fragmentation by electron impact of the gaseous products.

The hydroxyl radical, not NH_3, is believed to account for the m/e value of 17 (Table 7). Ammonia is known to be thermally unstable above 400 C, particularly in the presence of oxygen and/or hydrogen atoms (Ref. 8). In addition, the current studies have shown no NH_3 from HMX pyrolysis at ~800 C (Table 11). The expected m/e ratio of 18 to 17 for H_2O is approximately 5 to 1. The ratios found for HMX (Table 7), ring labeled N^{15} (Table 8), and total N^{15} labeled HMX (Table 9) are all significantly smaller, suggesting some OH formation during the HMX primary or secondary thermal decomposition and not all from mass fragmentation of H_2O by electron impact.

TABLE 10. MASS FRAGMENTATION PATTERNS OF GAS-PHASE COMPONENTS FROM HMX DECOMPOSITION (RELATIVE INTENSITY)

GAS PHASE COMPONENT	*MASS NUMBERS* 12	13	14	15	16	17	18	19	20	26	27	28	29	30	31	32	44	45	46	INTENSITY WITH RESPECT TO C-B. AVG
N₂			5	2	2							100	0.7		0.4	0.2				0.64
NO			3	0.1	5								0.1	100	0.1					0.78
N₂O			13	3	30	100	0.4					11		37			100	3.7	0.2	0.60
NH₃			2		22	100														0.32
NO₂			10	0.1						16			0.1	100					37	0.17
HCN	4	2	2	0.1	2					16	100	2	1	0.2						0.82
CO	5	0.1	1		9							100	1							0.77
CO₂	7								0.3		0.3	9	0.1	66			100			0.80
CH₂O		3	6	72	100	1	100	0.5				39	100	66						–
CH₄		1		6	100	21	36	0.3				72	0.3	100	31	0.7	66	0.3		0.37
H₂O	6	1	14	6	1	9	36													–
HMX (THEORETICAL AT 800 C)	6	1	14	6	9	9	36	0.3	0.3	6	39	72	0.3	100	31	0.7	66	0.3		–

*ONLY RELEVANT MASS NUMBERS ARE SHOWN

TABLE 11.   GASEOUS PRODUCT DISTRIBUTION FROM HMX PYROLYSIS
(~800 C, 10 SECONDS, 2 ATM HELIUM)

PRODUCT	WEIGHT PERCENT YIELD	MOLE PERCENT YIELD FROM N	MOLE PERCENT YIELD FROM C
N_2	10	26	
NO	30	37	
N_2O	11	18	
NH_3	0	0	
HCN	13	18	36
CO	12		32
CO_2	11		18
CH_2O	0		0
CH_4	<1		<5
H_2	<1		
H_2O	12		
	99	99	86

The m/e ratio of 27 (Table 7) can be accounted for only by HCN. It was con-
cluded earlier that HCN formation may be a rate-controlling process, partic-
ularly at low temperatures (~300 C).

The m/e ratio of 28 is attributed to CO, N_2, and CH_2N with the first two
being major gaseous products from the decomposition of HMX at ~800 C
(Table 11).

The assignments made for m/e value of 29 are to the species CH_2NH or CH_3N, and not CHO because the latter, formed from formaldehyde, is known to undergo highly exothermic gas-phase reaction with oxides of nitrogen (Ref. 9). Confirmation for the m/e assignment to CH_2NH or CH_3N intermediates is given by the presence of a m/e value of 29 (CH_2N^{15}) for the pyrolysis of totally N^{15} labeled HMX (Table 9). The possibility exists that these species can serve as precursors for HCN via further hydrogen abstraction. The relative intensity (24) for these species is significant (Table 7).

The m/e ratio of 30 (Table 7) is assigned to NO, which is the major HMX decomposition product at ~800 C. As previously mentioned, CH_2O is an unlikely species due to its high reactivity toward nitrogen oxides. The m/e value of 31, listed in Table 8, obtained from the pyrolysis of ring N^{15} labeled HMX, confirms the earlier conclusion that the majority of the NO is derived from the NO_2 nitrogens.

The m/e values of 39 to 43 may be due to a variety of CNH fragments as shown in Tables 7 through 9. Of particular interest is the m/e ratio of 43 with a relative intensity of 20 obtained for unlabeled HMX (Table 7). Possible species are NCH_2NH or HOCN (cyanic acid). The species NCH_2NH seems unlikely due to the lack of a similar intensity for a m/e ratio of 45, $N^{15}CH_2N^{15}H$, from the pyrolysis of totally N^{15} labeled HMX (Table 9). Cyanic acid boils at 23.5 C at atmospheric pressure and is a corrosive, very unstable liquid. It polymerizes spontaneously to form cyamelide $(CNOH)_x$ and cyanuric acid:
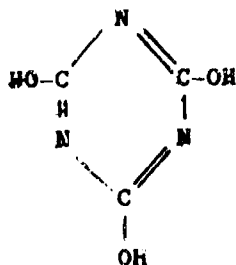
The proportion of cyanuric acid increases with temperature (Ref. 10). Above 360 C, cyanuric acid undergoes decomposition. Cyanic acid may be the source then of the polymeric residues observed from HMX decomposition reported by numerous investigators, particularly at low temperatures.

The m/e ratio of 44 (Table 7) is attributed to N_2O, CO_2, and/or CH_2NO; the first two compounds are major gaseous products from the pyrolysis of HMX at ~800 C (Table 11). Additional confirmation for N_2O was obtained from the pyrolysis of totally N^{15} labeled HMX, which resulted in a m/e value of 46 for $N^{15}O$ (Table 9).

The reduction of NO by NH_3 to N_2O involves an intermediate HNNO (Ref. 8). The m/e value of 45, therefore, may be an indication of the presence of this intermediate.

Nitrogen dioxide accounts for the observed m/e ratio of 46. Under the thermal conditions used, a major amount of any NO_2 formed would not be expected to survive, thereby resulting in the observed low relative intensity (Table 7). At temperatures <140 C, NO_2 decomposes to NO and O_2 and the reaction is quantitative above 600 C. In addition, NO_2 can undergo various gas phase reactions such as the following (Ref. 9), which result in the products observed in this study:

$$\Delta H, \text{ kcal/mole}$$

$$NO_2 + H \overset{\rightarrow}{\leftarrow} NO + OH \qquad\qquad -28.9$$

$$NO_2 + O \overset{\rightarrow}{\leftarrow} NO + O_2 \qquad\qquad -45.9$$

$$NO_2 + HCO \overset{\rightarrow}{\leftarrow} NO + H + CO_2 \qquad\qquad -33.7$$

$$NO_2 + HCO \overset{\rightarrow}{\leftarrow} HONO + CO \qquad\qquad -63.0$$

$$NO_2 + HCHO \overset{\rightarrow}{\leftarrow} HONO + HCO \qquad\qquad 11.4$$

$$NO_2 + NO_2 \overset{\rightarrow}{\leftarrow} 2NO + O_2 \qquad\qquad 27.3$$
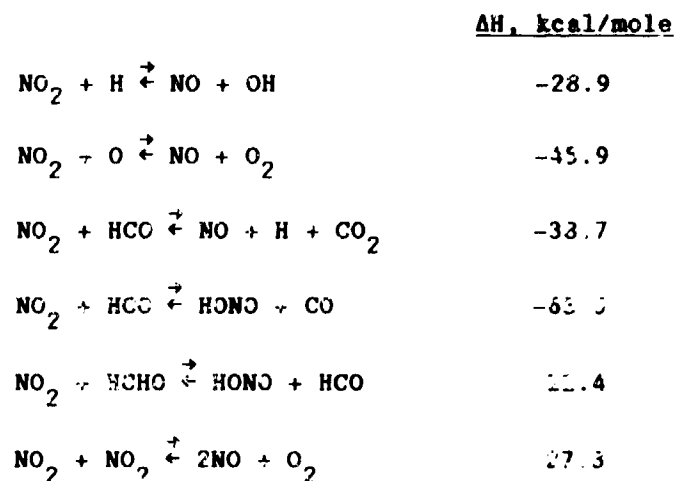
EFFECT OF ENERGETIC ADDITIVES ON HMX DECOMPOSITION

The effect of various energetic additives on the decomposition mechanism of HMX and its gaseous decomposition products was determined. The approach used was to determine any significant deviations between the experimental and theoretically predicted quantities of the gaseous products. If such deviations were observed, it could be concluded that the decomposition gases of the additive underwent a chemical and/or thermal interaction with those of HMX. In addition, a knowledge of the decomposition mechanism of the energetic additives and their interaction in the decomposition of HMX should lead to a better understanding of nitramine decomposition.

Premixed samples were prepared of HMX and the additive. The pyrolysis of the mixtures was conducted under 2 atm of helium at a maximum heating rate of approximately 850 C per second and held for 10 seconds in all experiments.

Pyrolysis of Triaminoguanidine Nitrate (TAGN)

Pure TAGN was pyrolyzed at ~800 and ~400 C, and the gaseous product distributions obtained are summarized in Tables 12 and 13, respectively. At the higher temperature, N_2 was the major nitrogen-containing product and no NH_3 was noted. When the pyrolysis was performed at the lower temperature, N_2 was again the major product but, in addition, a significant amount of NH_3 (20 m/o) also was noted.

Thermal Decomposition of HMX/TAGN Mixtures

The gaseous product distribution obtained from the pyrolysis of an 80 HMX-20 TAGN w/o mixture at ~800 C is given in Table 14. An analysis was performed on the degree of interaction between HMX and TAGN. This consisted of a comparison of the measured gas yields with those predicted (numbers in parentheses) by addition of the weighted product distributions from pure HMX and TAGN pyrolyzed under similar conditions. The key deviations noted in this analysis were those for N_2 and NO (Table 14.

TABLE 12. GASEOUS PRODUCT DISTRIBUTION FROM TAGN PYROLYSIS
(~800 C, 10 SECONDS, 2 ATM HELIUM)

PRODUCT	WEIGHT PERCENT YIELD	MOLE PERCENT YIELD FROM N	MOLE PERCENT YIELD FROM C
N_2	55	94	
NO	1	1	
N_2O	.1	.1	
NH_3	0	0	
HCN	5	4	31
CO	7		42
CO_2	9		34
CH_2O	0		0
CH_4	0		0
H_2	1		
H_2O	21		
	99	98	107

TABLE 13. GASEOUS PRODUCT DISTRIBUTION FROM TAGN PYROLYSIS
(~400 C, 10 SECONDS, 2 ATM HELIUM)*

PRODUCT	WEIGHT PERCENT YIELD	MOLE PERCENT YIELD FROM N	MOLE PERCENT YIELD FROM C
N_2	46	78	
NO	1	.1	
N_2O	6	6	
NH_3	14	20	
HCN	1	.1	6
CO	4		24
CO_2	13		49
CH_2O	0		0
CH_4	.		10
H_2	0		
H_2O	13		
	98	104	79
*THE SAMPLE WAS 75% PYROLYZED			

26

TABLE 14. PRODUCT DISTRIBUTION FROM 80 HMX-20 W/O TAGN PYROLYSIS
(~800 C, 10 SECONDS, 2 ATM HELIUM)

PRODUCT	WEIGHT PERCENT YIELD	MOLE PERCENT YIELD FROM N	MOLE PERCENT YIELD FROM C
N_2	22	52 (40)*	
NO	20	22 (30)	
N_2O	11	17 (14)	
NH_3	0	0 (0)	
HCN	10	12 (15)	31 (35)
CO	12		36 (34)
CO_2	12		23 (21)
CH_2O	0		0 (0)
CH_4	<1		<5 (5)
H_2	<1		
H_2O	12		
	99	103	90

*VALUES IN PARENTHESES ARE THOSE PREDICTED BASED ON
WEIGHTED GASEOUS PRODUCT DISTRIBUTIONS FROM PURE
HMX AND TAGN

Miller et al (Ref. 8) recently developed a chemical kinetic model that
explains the important features of the exothermic reduction of NO by NH_3 in
the presence of oxygen. Essential to the model is a mechanism that involves
the reduction of NO by amidogen (NH_2), which is formed from NH_3. The NO
reduction is most effective between 700 and 1000 C. At temperatures above
1200 C, the process becomes counterproductive and results in nonreduction of
NO. Hydrogen lowers the effective temperature region by ~5%. In addition,
OH radicals accelerate the conversion of NH_3 to NH_2. However, an excess
of OH radicals was found to have an inhibiting effect on the reduction of NO
by NH_3, particularly at temperatures >1200 C.

The current studies on the decomposition of HMX at ~800 C have shown that NO is a major product, while NH_3 is a product of the pyrolysis at ~300 C, but none is observed at ~800 C. Furthermore, there is experimental evidence that OH radicals and H_2 are products of the decomposition of HMX (Vacuum Decomposition of Isotopically Labeled and Unlabeled HMX Section). Thus, based on Miller's kinetic model, an optimum environment exists for NO reduction except for the presence of NH_2-type intermediates. This suggests that the combustion of HMX might be modified by the incorporation of additives which, on decomposition, would yield these types of species.

The generation of N_2 and H_2O in high yields and NO in a much lower amount during the pyrolysis of TAGN (Table 12) implies that NO is being reduced by NH_3 formed during the thermal decomposition process. Therefore, since this appears to be the case, it is not surprising that there was no dramatic deviation between the observed and predicted NO values (Table 14). An additive capable of generating NH_2 intermediates, but which contains little or no oxygen, would be a more effective ingredient for promoting chemical interactions with the HMX generated NO.

Bistriaminoguanidinium Azobitetrazole (TAGZT)

The compound TAGZT is quite similar to TAGN except that it contains no oxygen. TAGZT was pyrolyzed at ~800 C and, as expected, a much larger amount (16 m/o) of NH_3 was measured (Table 15).

Pyrolysis of HMX-TAGZT Mixtures

The first series of pyrolyses were conducted on a mixture of 80 HMX (ring labeled N^{15}) and 20 w/o TAGZT to establish the extent of NO reduction by the cogenerated NH_3 and/or its NH_2 derivative. The gaseous product distributions, including the N^{15}-labeled products, are given in Tables 16 and 17. As before, a comparison was made of the predicted and experimentally found quantities of the products to determine the extent of interaction. The principal finding from this analysis was a major reduction in the amount of NO theoretically expected and a doubling of the amount of N_2. In concert with this results, larger yields of CO and CO_2 were observed.

**TABLE 15. PRODUCT DISTRIBUTION FROM TAGZT PYROLYSIS
(~800 C, 1.0 SECONDS, 2 ATM HELIUM)***

PRODUCT	WEIGHT PERCENT YIELD	MOLE PERCENT YIELD FROM N	MOLE PERCENT YIELD FROM C
N_2	62	75	
NO	<1	0	
N_2O	<1	0	
NH_3	16	16	
HCN	15	9	52
CO	<1		0
CO_2	<1		0
CH_2O	0		0
CH_4	1		6
H_2	1		
H_2O	1		
	96	100	58

*APPROXIMATELY 90% OF THE SAMPLE WAS PYROLYZED
UNDER THESE CONDITIONS.

TABLE 16. PRODUCT DISTRIBUTION FROM 80 HMX (RING N^{15})-20 W/O TAGZT PYROLYSIS (~800 C, 10 SECONDS, 2 ATM HELIUM)

PRODUCT	WEIGHT PERCENT YIELD	MOLE PERCENT YIELD FROM N	MOLE PERCENT YIELD FROM C
N_2	32	68 (32)*	
NO	13	13 (34)	
N_2O	7	9 (14)	
NH_3	0	0 (3)	
HCN	9	10 (15)	25 (38)
CO	16		44 (26)
CO_2	14		25 (15)
CH_2O	0		0 (0)
CH_4	<1		<5 (<5)
H_2	1		
H_2O	8		
	100	100	94

*VALUES IN PARENTHESES ARE THOSE PREDICTED BASED ON WEIGHTED CONTRIBUTIONS OF THE PURE COMPOUNDS.

TABLE 17. LABELED PRODUCT DISTRIBUTION FROM 80 HMX (RING N^{15})- 20 W/O TAGZT PYROLYSIS (~800 C, 10 SECONDS, 2 ATM HELIUM)

LABELED PRODUCT	MASS NO.	RELATIVE PERCENT INTENSITY	MOLE PERCENT CONTRIBUTION FROM TOTAL N	MOLE PERCENT YIELD FROM TOTAL N
$N^{14} N^{14}$	28	50	34	
$N^{15} N^{14}$	29	45	31	68 (32)*
$N^{15} N^{15}$	30	5	3	
$N^{14} O$	30	95	12	13 (34)
$N^{15} O$	31	5	1	
$N^{14}=N^{14}-O$	44	0	0	
$N^{15}=N^{14}-O$	45	98	9	9 (14)
$N^{15}=N^{15} O$	46	2	1	
HC N^{14}	27	30	3	10 (15)
HC N^{15}	28	70	7	

*VALUES IN PARENTHESES ARE THOSE PREDICTED BASED ON WEIGHTED CONTRIBUTIONS OF THE PURE COMPOUNDS.

Analyses of the results shown in Table 17, when compared to those presented in Table 6, support the hypothesis that NH_3-derived intermediates can indeed interact with the decomposition gases of HMX. For example, the N_2 consisted of nearly equal amounts of $N^{14}N^{14}$ and $N^{15}N^{14}$, as compared to essentially pure $N^{15}N^{14}$ when neat ring labeled N^{15} was used. Since it was observed that this type of isotopically labeled HMX gave primarily $N^{14}O$ when pyrolyzed (Table 6), the N_2 isotopic mixture observed from the decomposition of the HMX-TAGZT sample must have resulted from the interaction of the $N^{14}O$ with $N^{14}H_{3-X}$ from the TAGZT. Further substantiation of this mechanism is the fact that the observed quantity of $N^{14}N^{14}$ could not have come from the TAGZT alone.

The effectiveness of TAGZT on the reduction of NO generated from HMX was further tested by pyrolysis of a 60 HMX–40 w/o TAGZT mixture under similar conditions (Table 18). In this case, the NO yield was reduced by a factor of 3 and the N_2 yield increased by a factor less than 2. (The smaller N_2 increase was due to the greater quantity of TAGZT in the mixture.)

TABLE 18.   PRODUCT DISTRIBUTION FROM 60 HMX–40 W/O TAGZT PYROLYSIS
(~800 C, 10 SECONDS, 2 ATM HELIUM)

PRODUCT	WEIGHT PERCENT YIELD	MOLE PERCENT YIELD FROM N	MOLE PERCENT YIELD FROM C
N_2	41	74 (46)*	
NO	8	7 (2.5)	
N_2O	9	10 (11)	
NH_3	6	9 (6)	
HCN	11	9 (14)	11 (27)
CO	15		25 (39)
CO_2	15		4 (11)
CH_2O	2		5 (3)
CH_4	1		3 (3)
H_2	1		
H_2O	5		
	103	10	80

*VALUES IN PARENTHESES ARE THOSE PREDICTED BASED ON WEIGHTED CONTRIBUTIONS OF THE SEPARATE INGREDIENTS.

The above test results indicated the potential attributes of TAGZT for modifying the combustion of HMX, which was demonstrated further during burning rate studies on propellants containing this ingredient (see Combustion Rate Studies section).

In conclusion, a summary of those factors that influence the effectiveness of the exothermic HMX-NO reduction by additive NH_2 intermediates, as determined by this study and those referenced, is given below:

1. The effective temperature region of the exothermic NO reduction to N_2 by NH_2 intermediates is ~700 to 1200 C (Ref. 11)
2. The concentration ratio of NH_3 to NO is critical
3. Diffusional gradients may be the most important factor, thus, additive particle size is very important
4. Matching of additive and nitramine decomposition temperature
5. Rate of additive decomposition
6. Self-consumption of NH_2 by the additive itself, thus negating chemical interaction with HMX-NO (TAGN decomposes in such a manner)

Bisdiammonium Azobitetrazole (DAZT)

This compound is the diammonium analog of TAGZT. Pyrolysis studies were conducted on neat DAZT and HMX-DAZT mixtures to determine the extent of interaction of the gaseous decomposition products.

The gaseous products and their amounts from the decomposition of DAZT are summarized in Table 19. This compound, unlike TAGZT, exploded upon initiation of the pyrolysis. Nitrogen was a major product (66 m/o) and hydrazine (27 m/o), not found as a decomposition product of TAGZT, was formed at a higher level than NH_3 (9 m/o). A possible explanation for the formation of N_2H_4 in such quantities may be due to coupling reactions of NH_2 radicals produced by the decomposition of NH_3 generated during the pyrolysis of DAZT.

TABLE 19. PRODUCT DISTRIBUTION FROM DAZT PYROLYSIS*
(~800 C, 10 SECONDS, 2 ATM HELIUM)

PRODUCT	WEIGHT PERCENT YIELD	MOLE PERCENT YIELD FROM N	MOLE PERCENT YIELD FROM C
N_2	55	66	
NO	0	0	
N_2O	0	0	
NH_3	4	4	
N_2H_4	26	27	
HCN	10	6	17
CO	0		0
CO_2	0		0
CH_2O	0		0
CH_4	0		0
H_2	1		
H_2O	0		
	100	108	37

*EXPLODES UNDER THESE PYROLYSIS CONDITIONS

Pyrolysis of HMX-DAZT Mixture

Pyrolysis studies were conducted on an 80 HMX-20 w/o DAZT mixture and the products identified and quantified (Table 20) On occasion, this mixture detonated during the pyrolysis. In those instances, no significant differences were noted in the nature or quantity of the products.

As observed for the HMX-TAGZT mixture, the addition of DAZT to HMX resulted in a significant decrease in the theoretically predicted yield of NO and an increase in the N_2 yield. The NH_3 yield was reduced to 0%, whereas the N_2H_4 did not appear to undergo any oxidation during the pyrolysis. Otherwise, the product distribution was similar to that previously reported for the 80 HMX-20 w/o TAGZT mixture (Table 16)

PRODUCT	WEIGHT PERCENT YIELD	MOLE PERCENT YIELD FROM N	MOLE PERCENT YIELD FROM C
N_2	27	57 (34)*	
NO	13	13 (30)	
N_2O	9	12 (14)	
NH_3	0	6 (2)	
N_2H_4	5	9 (5)	
HCN	6	7 (16)	17 (36)
CO	11		13 (26)
CO_2	19		34 (14)
CH_2O	0		0 (0)
CH_4	0		0 (-4)
H_2	-1		
H_2O	10		
	100	98	82

*VALUES IN PARENTHESES ARE WEIGHTED AMOUNTS OF THE
EXPECTED GASES ASSUMING NO INTERACTION

Ammonium 5-Nitraminotetrazole (ANAT)

The chemical composition of ANAT provides an equimolar balance of nitramine
and ammonium groups so that one might expect a quantitative reduction of the
NO by NH_3, both generated by the decomposition of ANAT. The decomposition
gases formed during the pyrolysis of ANAT at 800 C are summarized in
Table 21. The principal results were a high yield (89 m/o) of N_2 and a
very low yield (3 m/o) of NO, as was expected from the chemical interaction
between NO and NH_3.

Pyrolysis of HMX-ANAT Mixture

The effect of ANAT on the decomposition of HMX was measured on a 80 HMX-20
w/o ANAT mixture. The results, summarized in Table 22, again demonstrated
that additives containing moieties capable of generating NH_3, and from it
NH_2-type intermediates, can reduce significantly the theoretical yield of
NO by a chemical interaction.

TABLE 21. PRODUCT DISTRIBUTION FROM ANAT PYROYLYSIS
(~800 C, 10 SECONDS, 2 ATM HELIUM)

PRODUCT	WEIGHT PERCENT YIELD	MOLE PERCENT YIELD FROM N	MOLE PERCENT YIELD FROM C
N_2	60	89	
NO	5	3	
N_2O	1	1	
NH_3	0	0	
N_2H_4	2	3	
HCN	6	5	32
CO	5		31
CO_2	7		23
CH_2O	0		0
CH_4	1		9
H_2	1		
H_2O	13		
	100	101	86

TABLE 22. PRODUCT DISTRIBUTION FROM 80 HMX-20 W/O ANAT PYROLYSIS
(~800 C, 10 SECONDS, 2 ATM HELIUM

PRODUCT	WEIGHT PERCENT YIELD	MOLE PERCENT YIELD FROM N	MOLE PERCENT YIELD FROM C
N_2	26	60 (39)*	
NO	19	20 (30)	
N_2O	9	13 (15)	
NH_3	0	0 (0)	
N_2H_4	0	0 (1)	
HCN	8	5 (15)	24 (35)
CO	12		35 (32)
CO_2	14		26 (19)
CH_2O	0		0 (0)
CH_4	1		3 (5)
H_2	1		
H_2O	2		
	100	102	85

*THE VALUES IN PARENTHESES ARE THOSE PREDICTED BASED ON WEIGHTED AMOUNTS DERIVED FROM THE EXPECTED YIELDS OF THE INDIVIDUAL COMPONENTS.

1,7-Diazido-2,4,6-Trinitrazaheptane (DATH)

DATH is an azido containing nitramine and it was investigated to determine the effect of the azido group on the decomposition of the nitramine moiety. The results obtained on the pyrolysis of neat DATH, summarized in Table 23, strongly suggest a significant influence of the azide group on the nitramine decomposition mechanism of DATH.

TABLE 23.   PRODUCT DISTRIBUTION FROM DATH PYROLYSIS
(~800 C, 10 SECONDS, 2 ATM HELIUM)

PRODUCT	WEIGHT PERCENT YIELD	MOLE PERCENT YIELD FROM N	MOLE PERCENT YIELD FROM C
N_2	45	86	
NO	4	4	
N_2O	3	4	
NH_3	0	0	
HCN	4	4	12
CO	25		71
CO_2	11		20
CH_2O	0		0
CH_4	1		5
H_2	1		
H_2O	7		
	100	98	103

Pyrolysis of N^{15} Labeled DATH

Isotopically labeled DATH, with the center nitrogen of the azide group N^{15} labeled, was prepared from $NaNN^{15}N$ and pyrolyzed under the standard conditions to gain a better understanding of the azide-nitramine interaction. A comparison of the results, summarized in Tables 23 and 24, shows that the product distributions are near identical. Mass spectrometer analyses were performed on the decomposition gases from the labeled DATH (Table 25), which indicated that the N_2 consisted of $N^{15}N^{14}$ and $N^{14}N^{14}$ in a ratio of 1/3 to 2/3, respectively. This indicates that both azide groups of DATH

TABLE 24. PRODUCT DISTRIBUTION FROM PYROLYSIS OF CENTER N^{15} LABELED DATH (~800 C, 10 SECONDS, 2 ATM HELIUM)

PRODUCT	WEIGHT PERCENT YIELD	MOLE PERCENT YIELD FROM N	MOLE PERCENT YIELD FROM C
N_2	47	89	
NO	3	3	
N_2O	3	4	
NH_3	0	0	
HCN	3	3	9
CO	27		77
CO_2	11		20
CH_2O	0		0
CH_4	·1		·5
H_2	1		
H_2O	5		
	100	99	106

TABLE 25. LABELED (N^{15}) PRODUCT DISTRIBUTION FROM PYROLYSIS OF CENTER N^{15} LABELED DATH (~800 C, 10 SECONDS, 2 ATM HELIUM)

LABELED PRODUCT	MASS NO.	RELATIVE PERCENT INTENSITY	MOLE PERCENT CONTRIBUTION FROM TOTAL N	MOLE PERCENT YIELD FROM TOTAL N
$N^{14} \equiv N^{14}$	28	65	58	
$N^{15} \equiv N^{14}$	29	35	31	89
$N^{15} \equiv N^{15}$	30	0	0	
$N^{14} = 0$	30	90	2	
$N^{15} = 0$	31	10	·1	3
$N^{14} = N^{14} = 0$	44	85	3	
$N^{15} = N^{14} = 0$	45	15	·1	3
$N^{15} = N^{15} = 0$	46	0	0	
$HC \equiv N^{14}$	27	100	3	
$HC \equiv N^{15}$	28	0	0	3

37

decompose via N_2 evolution, which results in the observed $N^{15}N^{14}$ yield of 31 m/o. The $N^{14}N^{14}$ then must be the decomposition product of the N-NO$_2$ group. The oxygen present in the NO$_2$ groups result in high yields of CO and CO_2.

The pyrolysis of N^{15} labeled DATH also was investigated at a temperature slightly above its melting point(~140 C). Based on the results obtained (Table 26), the C-N bond of DATH is less stable than the azide linkage. This conclusion is reached on the basis that N_2O was the major decomposition gas, rather than N_2, along with CH_2O. This observation is comparable to that previously discussed for HMX where C-N bond cleavage was faster than N-NO$_2$ bond rupture at ~300 C.

TABLE 26. PRODUCT DISTRIBUTION FROM PYROLYSIS OF CENTER N^{15} LABELED DATH AT ~140 C* (10 SECONDS, 2 ATM HELIUM)

PRODUCT	WEIGHT PERCENT YIELD	MOLE PERCENT YIELD FROM N	MOLE PERCENT YIELD FROM C
N_2	13	25	
NO	0	0	
N_2O	61	74	
NH_3	0	0	
HCN	0	0	0
CO	0		0
CO_2	2		4
CH_2O	20		54
CH_4	0		0
H_2	0		
H_2O	2	---	---
	98	99	58

*APPROXIMATELY 30% OF THE SAMPLE WAS PYROLYZED UNDER THESE CONDITIONS

decompose via N_2 evolution, which results in the observed $N^{15}N^{14}$ yield of 31 m/o. The $N^{14}N^{14}$ then must be the decomposition product of the $N-NO_2$ group. The oxygen present in the NO_2 groups result in high yields of CO and CO_2.

The pyrolysis of N^{15} labeled DATH also was investigated at a temperature slightly above its melting point(~140 C). Based on the results obtained (Table 26), the C-N bond of DATH is less stable than the azide linkage. This conclusion is reached on the basis that N_2O was the major decomposition gas, rather than N_2, along with CH_2O. This observation is comparable to that previously discussed for HMX where C-N bond cleavage was faster than $N-NO_2$ bond rupture at ~300 C.

TABLE 26.   PRODUCT DISTRIBUTION FROM PYROLYSIS OF CENTER N^{15} LABELED
DATH AT ~140 C* (10 SECONDS, 2 ATM HELIUM)

PRODUCT	WEIGHT PERCENT YIELD	MOLE PERCENT YIELD FROM N	MOLE PERCENT YIELD FROM C
N_2	13	25	
NO	0	0	
N_2O	61	74	
NH_3	0	0	
HCN	0	0	0
CO	0		0
CO_2	2		4
CH_2O	20		54
CH_4	0		0
H_2	0		
H_2O	2		
	98	99	58
*APPROXIMATELY 30% OF THE SAMPLE WAS PYROLYZED UNDER THESE CONDITIONS			

33

While the pyrolysis of DATH was only ~30% at 140 C, its decomposition at ~160 C was quantitative. The product distribution at this temperature (Table 27) was quite similar to that observed at ~800 C (Table 23).

TABLE 27. PRODUCT DISTRIBUTION FROM PYROLYSIS OF CENTER N^{15} LABELED DATH AT ~160 C (10 SECONDS, 2 ATM HELIUM)

PRODUCT	WEIGHT PERCENT YIELD	MOLE PERCENT YIELD FROM N	MOLE PERCENT YIELD FROM C
N_2	44	83	
NO	7	6	
N_2O	9	11	
NH_3	0	0	
HCN	3	3	9
CO	22		63
CO_2	9		16
CH_2O	0		0
CH_4	1		5
H_2	1		
H_2O	5		
	100	103	88

Pyrolysis of HMX-DATH Mixture

Mixtures of HMX and unlabeled DATH (80 and 20 w/o, respectively) were pyro-lyzed at ~300 and ~800 C. The studies conducted at the lower temperature gave a higher NO but lower N_2O yield than those predicted from the theoretical yields of the individual reactants (Table 28). The pyrolysis results obtained at ~800 C (Table 29) were more in line with those expected assuming no chemical interaction between the product gases. The conclusion reached from these studies is that, unlike the previously discussed additives, which can generate NH_3 and its dissociation species, any acceleration in the decomposiiton of HMX by DATH will result via the exothermic decomposition of the azide group and not by chemical interactions of the product gases.

TABLE 28. PRODUCT DISTRIBUTION FROM 80 HMX-20 W/O DATH PYROLYSIS*
(~300 C, 10 SECONDS, 2 ATM HELIUM)

PRODUCT	WEIGHT PERCENT YIELD	MOLE PERCENT YIELD FROM N	MOLE PERCENT YIELD FROM C
N_2	15	37 (37)**	
NO	24	28 (16)	
N_2O	20	31 (43)	
NH_3	0	0 (2)	
HCN	8	10 (1)	22 (2)
CO	11		29 (23)
CO_2	12		20 (18)
CH_2O	0		0 (22)
CH_4	<1		<5 (<4)
H_2	<		
H_2O	10	—	—
	100	106	71

*THE SAMPLE WAS APPROXIMATELY 80% PYROLYZED
**THE VALUES IN PARENTHESES ARE THOSE PREDICTED BASED
ON WEIGHTED AMOUNTS DERIVED FROM THE EXPECTED YIELDS
OF THE INDIVIDUAL COMPONENTS.

TABLE 29. PRODUCT DISTRIBUTION FRM 80 HMX-20 W/O DATH PYROLYSIS
(~800 C, 10 SECONDS, 2 ATM HELIUM)

PRODUCT	WEIGHT PERCENT YIELD	MOLE PERCENT YIELD FROM N	MOLE PERCENT YIELD FROM C
N_2	13	32 (38)*	
NO	25	29 (30)	
N_2O	13	20 (15)	
NH_3	0	0 (0)	
HCN	12	15 (15)	33 (31)
CO	12		32 (40)
CO_2	14		24 (18)
CH_2O	0		0 (0)
CH_4	<1		<5 (<5)
H_2	<1		
H_2O	10	—	—
	99	96	89

*THEORETICAL VALUES BASED ON WEIGHTED AMOUNTS DERIVED
FROM THE INDIVIDUAL COMPONENTS AND ASSUMING NO CHEMICAL
INTERACTIONS.

1-Azido-3,6-Dinitro-1,3,6-Triazacycloheptane (AMDTH)

The second azido-containing nitramine investigated during this series of studies was AMDTH. The products (and their amounts) from the pyrolysis of AMDTH are summarized in Table 30.

Pyrolysis of HMX/AMDTH Mixture

The behavior of AMDTH when admixed with HMX, 80 HMX-20 w/o AMDTH, was quite different than that exhibited by DATH in similar mixtures. The N_2 yield was appreciably greater and the NO yield significantly less than the values calculated on the basis of the pyrolysis product yields from the pure compounds (Table 31). These results strongly indicated that the attempts made to incorporate azide groups into the structure of HMX (subsequently discussed) might lead to changes in its combustion characteristics.

Azobisnitroformamidine (ABNF)

Neat ABNF burns at a very fast rate and, therefore, pyrolysis studies were conducted on it and a mixture with HMX. Based on the results shown in Table 32, its principal product gas is N_2 and the majority of the NO_2 oxygen is recovered as CO and CO_2.

Pyrolysis of HMX-ABNF Mixture

No apparent significant interactions occurred between the product gases from the pyrolysis of a 80-20 w/o HMX-ABNF mixture at 800 C (Table 33). Analyses of the gases gave a product distribution quite similar to that predicted based on the pure compounds.

Cyanoguanidine

Cyanoguanidine was found to give a high yield of NH_3 when pyrolyzed at ~800 C (Table 34). However, the extent of pyrolysis was quite low (~20%) under these conditions which indicates its high thermal stability in the absence of oxygen. Since the thermal decomposition was limited, no studies were conducted on mixtures of HMX with this material

PRODUCT	WEIGHT PERCENT YIELD	MOLE PERCENT YIELD FROM N	MOLE PERCENT YIELD FROM C
N_2	28	62	
NO	10	10	
N_2O	4	6	
NH_3	0	0	
HCN	13	15	24
CO	15		26
CO_2	19		21
CH_2O	0		0
CH_4	2		6
$CH_2=CH_2$	1		4
H_2	1		
H_2O	8		
	100	93	8?

*SAMPLE WAS 90 PYROLYZED

TABLE 31. PRODUCT DISTRIBUTION FROM 80 HMX-20 W/O AMDTH PYROLYSIS
(~800 C, 10 SECONDS, 2 ATM HELIUM)

PRODUCT	WEIGHT PERCENT YIELD	MOLE PERCENT YIELD FROM N	MOLE PERCENT YIELD FROM C
N_2	25	63 (33)*	
NO	10	12 (22)	
N_2O	7	11 (16)	
NH_3	0	0 (0)	
HCN	7	9 (17)	18 (34)
CO	23		55 (31)
CO_2	19		29 (19)
CH_2O	0		0 (0)
CH_4	1		4 (5)
$CH_2=CH_2$	1		2 (1)
H_2	1		
H_2O	9		
	100	95	102

*VALUES IN PARENTHESES ARE THEORETICAL AND WERE
CALCULATED ON THE BASIS OF THE EXPECTED PRODUCTS
FROM THE PURE COMPOUNDS.

42

TABLE 32. PRODUCT DISTRIBUTION FROM ABNF PYROLYSIS*
(~800 C, 10 SECONDS, 2 ATM HELIUM)

PRODUCT	WEIGHT PERCENT YIELD	MOLE PERCENT YIELD FROM N	MOLE PERCENT YIELD FROM C
N_2	45	82	
NO	3	3	
N_2O	7	8	
NH_3	0	0	
HCN	<1	<1	<3
CO	13		47
CO_2	26		60
CH_2O	0		0
CH_4	0		
H_2	<1		
H_2O	6		
	100	94	107

*THE SAMPLE WAS 90% PYROLYZED

53

TABLE 33. PRODUCT DISTRIBUTION FROM 80 HMX-20 W/O ABNF PYROLYSIS
(~800 C, 10 SECONDS, 2 ATM HELIUM)

PRODUCT	WEIGHT PERCENT YIELD	MOLE PERCENT YIELD FROM N	MOLE PERCENT YIELD FROM C
N_2	15	36 (37)*	
NO	23	26 (30)	
N_2O	19	29 (16)	
NH_3	0	0 (0)	
HCN	8	10 (14)	23 (29)
CO	9		25 (35)
CO_2	17		30 (26)
CH_2O	0		0 (0)
CH_4	<1		<5 (<4)
H_2	<1		
H_2O	8		
	99	101	78

*VALUES IN PARENTHESES ARE ADDITIVE THEORETICAL

TABLE 34. PRODUCT DISTRIBUTION FROM CYANOGUANIDINE PYROLYSIS*
(~800 C, 10 SECONDS, 2 ATM HELIUM)

PRODUCT	WEIGHT PERCENT YIELD	MOLE PERCENT YIELD FROM N	MOLE PERCENT YIELD FROM C
N_2	17	25	
NO	0	0	
N_2O	0	0	
NH_3	58	72	
HCN	22	17	34
N_2H_4	2	3	
CO	<1		0
CO_2	0		0
CH_2O	0		0
CH_4	<1		3
H_2	0		
H_2O	<1		
	99	117	34

*SAMPLE WAS 20% PYROLYZED

Cupric Diammonium-Diazide Complex [Cu(NH$_3$)$_2$(N$_3$)$_2$]

Table 35 summarizes the gas-phase product distribution from the pyrolysis of [Cu(NH$_3$)$_2$(N$_3$)$_2$] at ~800 C for 10 seconds under 2 atmospheres helium. The N$_2$ and NH$_3$ yields (43 and 18 weight percent, respectively), were close to that theoretically expected. Elemental analysis for copper (36 weight percent) was also close to theoretical. The compound undergoes a violent detonation at 210 C. Thus, the highly exothermic generation of significant NH$_3$ yields without the presence of oxygen (to prevent self-oxidation of NH$_3$) made [Cu(NH$_3$)$_2$(N$_3$)$_2$] a viable candidate as an additive for exothermic gas-phase HMX-NO reduction to N$_2$.

TABLE 35. PRODUCT DISTRIBUTION FROM PYROLYSIS OF
[Cu(NH$_3$)$_2$(N$_3$)$_2$] AT ~800 C, 10 SECONDS, 2 ATM HELIUM

PRODUCT	WEIGHT PERCENT YIELD	MOLE PERCENT YIELD FROM N
N$_2$	43	70
NO	<1	<1
N$_2$O	<1	<1
NH$_3$	18	24
HCN	0	0
CO	<1	
CO$_2$	1	
CH$_2$O	0	
CH$_4$	0	
H$_2$	0	
H$_2$O	1	
Cu	36	
	99	94

Table 36 gives the gas-phase product distribution from pyrolysis of a 95 HMX-5[Cu(NH$_3$)$_2$(N$_3$)$_2$] weight percent mix at ~800 C for 10 seconds under 2 atmospheres helium. A comparison of mole percent yields of gaseous products determined experimentally with those expected theoretically (values in parentheses), based on weighted amounts of the individual components, show an increase in N$_2$O and decrease in HCN. Thus, the expected HMX-NO reduction to N$_2$ via NH$_2$ intermediates from [Cu(NH$_3$)$_2$(N$_3$)$_2$] did not occur. It is believed that the significant decomposition temperature difference between HMX (280 C) and [Cu(NH$_3$)$_2$(N$_3$)$_2$] (210 C) in addition to the very rapid decomposition/deflagration of [Cu(NH$_3$)$_2$(N$_3$)$_2$] prevents adequate chemical and/or thermal interaction. To test this hypothesis, the gas-phase product distribution from the pyrolysis of a 95RDX-5 w/o [Cu(NH$_3$)$_2$(N$_3$)$_2$] mixture was determined as shown in Table 37. RDX, which undergoes thermal decomposition at 201 C, would be expected to undergo a greater chemical and/or thermal interaction with [Cu(NH$_3$)$_2$(N$_3$)$_2$] than that found with HMX based on the similarity in decomposition temperatures. As the data of Table 37 illustrate, this was indeed the case. Three-fourths (77 mole percent) of the total available nitrogen was found as N$_2$ with NO and N$_2$O yields decreased significantly (7 and 5 mole percent, respectively) from that expected. In addition, it can be seen that the majority of oxygen was utilized to produce CO and CO$_2$, resulting in total carbon oxidation. Thus, a major factor was identified in obtaining a significant chemical and/or thermal interaction with HMX or RDX with additives, that of matching the nitramine and additive decomposition temperatures, particularly when the additive undergoes very rapid decomposition.

Triaminoguanidinium-5-Aminotetrazole (TAG·5AT)

Table 38 gives the gas phase product distribution from the pyrolysis of TAG·5AT at ~800 C for 10 seconds under 2 atmospheres helium. Of particular interest is the high NH$_3$ yield (38 weight percent) found in the pyrolysis of this oxygen-free energetic compound. This is considerably higher than the NH$_3$ yield from the previously studied TAGZT (16 weight percent). However, the relatively low 42 mole percent total carbon yield from pyrolysis of TAG·5AT suggests a relatively high residue yield after pyrolysis and also

TABLE 36. PRODUCT DISTRIBUTION FROM 95 HMX-5 W/O $[Cu(NH_3)_2(N_3)_2]$ PYROLYSIS AT ~800 C, 10 SECONDS, 2 ATM HELIUM

PRODUCT	WEIGHT PERCENT YIELD	MOLE PERCENT YIELD FROM N	MOLE PERCENT YIELD FROM C
N_2	12	31(28)*	
NO	28	34(35)	
N_2O	16	26(17)	
NH_3	0	0(1)	
HCN	3	4(17)	9(34)
CO	11		31(30)
CO_2	17		30(17)
CH_2O	0		0(0)
CH_4	<1	--	<5(<5)
H_2	1		
H_2O	10		
Cu	2	------	------
	99	95	70

*THE VALUES IN PARENTHESES ARE THOSE PREDICTED BASED ON WEIGHTED AMOUNTS OF INDIVIDUAL COMPONENTS

TABLE 37. PRODUCT DISTRIBUTION FROM 95 RDX-5 W/O [Cu(NH$_3$)$_2$(N$_3$)$_2$] PYROLYSIS AT ~800 C, 10 SECONDS, 2 ATM HELIUM

PRODUCT	WEIGHT PERCENT YIELD	MOLE PERCENT YIELD FROM N	MOLE PERCENT YIELD FROM C
N$_2$	30	77(24)*	
NO	6	7(40)	
N$_2$O	3	5(21)	
NH$_3$	0	0(1)	
HCN	1	1(10)	3(21)
CO	20		52(30)
CO$_2$	28		50(21)
CH$_2$O	0		0(0)
CH$_4$	<1		<5(<5)
H$_2$	1		
H$_2$O	9		
Cu	2		
	100	90	105

*THE VALUES IN PARENTHESES ARE THOSE PREDICTED BASED ON WEIGHTED AMOUNTS OF INDIVIDUAL COMPONENTS

48

TABLE 38. PRODUCT DISTRIBUTION FROM TAG-SAT PYROLYSIS AT
~800 C, 10 SECONDS, 2 ATM HELIUM

PRODUCT	WEIGHT PERCENT YIELD	MOLE PERCENT YIELD FROM N	MOLE PERCENT YIELD FROM C
N_2	43	53	
NO	0	0	
N_2O	0	0	
NH_3	38	38	
HCN	12	8	42
CO	<1		<3
CO_2	0		0
CH_2O	0		0
CH_4	<1		<6
H_2	1		
H_2O	5		
	99	99	42

49

indicates an overall "cooling" effect during decomposition. This cooling effect may be the result of an excess of NH_3, which is known to behave as a flame retardant in high concentrations. TAG·5AT was found to burn in ambient air with the formation of a liquid pool below the flame zone.

Table 39 gives the gas phase product distribution from the pyrolysis of a 80 HMX–20TAG·5AT weight percent mix at ~300 C for 10 seconds under 2 atmospheres helium. The data show a decrease in NO and an increase in the N_2 yield from that theoretically expected. This implies HMX–NO reduction to N_2 occurred via TAG·5AT–NH_3, but not to the extent found with TAGZT. With TAG·5AT, the amount of carbon oxidation was as predicted (CO and CO_2 yields) with HMX. An increase in the amount of the theoretically derived N_2O (indicating the less exothermic HMX C–N bond scission occurred to a greater extent than the more exothermic N–NO_2 bond scission) also was observed. Finally, the slightly reduced total carbon yield (76%) from pyrolysis of the 80 HMX–20 w/o TAG·5AT mixture versus that from pure HMX (86%) also indicates a slight cooling effect caused by the greater amount of carbon residue formed during the pyrolysis. Thus, another factor influencing HMX/ additive interaction is the concentration ratio of NH_3 from the additive to NO from HMX. In addition, the decomposition temperature of 120 C for TAG·5AT is significantly lower than that of HMX (280 C) and generation of high NH_3 yields might be expected to have a flame-retarding effect.

Lithium and Sodium Azide

Recent burn rate studies at Morton-Thiokol have shown small concentrations of sodium azide have an effect on HMX burn rates. Thus, gas phase product distribution from the pyrolysis of 98 HMX–2 LiN_3 and 98 HMX–2 NaN_3 weight percent mixes at ~800 C for 10 seconds under 2 atmospheres helium were determined. Table 40 gives the data from these experiments. It can be seen that dramatic changes from the theoretical gas phase product yields are obtained with both LiN_3 and NaN_3. LiN_3 is reported to undergo measurable decomposition above 210 C in a highly irreproducible manner (Ref. 12).

TABLE 39. PRODUCT DISTRIBUTION FROM 80 HMX-20 TAG·5AT W/O
PYROLYSIS AT ~800 C, 10 SECONDS, 2 ATM HELIUM

PRODUCT	WEIGHT PERCENT YIELD	MOLE PERCENT YIELD FROM N	MOLE PERCENT YIELD FROM C
N_2	21	45(31)*	
NO	14	14(30)	
N_2O	18	25(14)	
NH_3	0	0(8)	
HCN	11	12(16)	32(37)
CO	10		28(26)
CO_2	9		16(14)
CH_2O	0		0(0)
CH_4	<1		<5(<5)
H_2	<1		
H_2O	15	———	——
	98	96	76

*THE VALUES IN PARENTHESES ARE THOSE PRE-
DICTED BASED ON WEIGHTED AMOUNTS OF INDI-
VIDUAL COMPONENTS

NaN_3 is reported to undergo rapid decomposition at temperatures above 370 C, with decomposition rates dependent on the specific surface area of NaN_3 crystals (Ref. 13). Upon decomposition, LiN_3 and NaN_3 evolve N_2 with the coproduction of the very reactive solid-state LiN and NaN radicals. These could be expected to behave as very active proton scavengers abstracting hydrogen from methylene groups (CH_2) about the HMX ring. This mechanism would account for the very low HCN yields found (Table 40) in these experiments. In addition, increased H_2 yields are indicative of a hydrogen abstraction process. Although both LiN_3 and NaN_3 appear to display a "catalytic" effect in altering the HMX decomposition mechanism, significant changes in HMX propellant burn rates were not encountered. It may be that intimate contact is lost between HMX and the active LiN or NaN intermediates in propellant mixes or that the overall change in decomposition mechanism is not improved substantially in terms of heat release generated.

RDX

Table 41 gives the gas phase product distribution from pyrolysis of RDX at ~220 C and ~800 C for 10 seconds under 2 atmospheres helium. In the low-temperature region just above liquefaction of RDX (201 C), the gas phase product distribution indicates a faster rate of RDX liquefaction to gasification. RDX undergoes 90% pyrolysis with comparable C-N and $N-NO_2$ bond scission occurring as given by the almost identical N_2O and NO yields, respectively. HMX undergoes only 70% pyrolysis just above the liquefaction region, giving higher N_2O than NO yields, indicating more C-N bond scission than $N-NO_2$ bond scission. This complements the recent work of Brill who has shown that crystal lattice interactions are greater in HMX than RDX, implying a faster rate of RDX gasification (Ref. 14).

TABLE 40. PRODUCT DISTRIBUTION FROM HMX-ALKALI AZIDE PYROLYSIS AT ~800 C, 10 SECONDS, 2 ATM HELIUM

PRODUCT	WEIGHT PERCENT YIELD	MOLE PERCENT YIELD FROM N	MOLE PERCENT YIELD FROM C	PRODUCT	WEIGHT PERCENT YIELD	MOLE PERCENT YIELD FROM N	MOLE PERCENT YIELD FROM C
N_2	40	77(27)*		N_2	40	78(27)*	
NO	6	7(36)		NO	9	11(36)	
N_2O	2	3(18)		N_2	4	7(18)	
NH_3	0	0(0)		NH_3	0	0(0)	
HCN	1	1(18)	3(35)	HCN	1	1(18)	3(35)
CO	20		54(31)	CO	21		57(31)
CO_2	27		46(18)	CO_2	21		36(18)
CH_2O	0		0(0)	CH_2O	5		0(0)
CH_4	<1		<5(<5)	CH_4	<1		<5(<5)
H_2	1			H_2	1		
H_2O	13			H_2O	13		
	100	88	103		100	97	96

*THE VALUES IN PARENTHESES ARE THOSE PREDICTED BASED ON WEIGHTED AMOUNTS OF INDIVIDUAL COMPONENTS.

TABLE 41. GASEOUS PRODUCT DISTRIBUTION FROM PYROLYSIS OF RDX (10 SECONDS, 2 ATM HELIUM)

	~220 C*				~800 C		
PRODUCT	WEIGHT PERCENT YIELD	MOLE PERCENT YIELD FROM N	MOLE PERCENT YIELD FROM C	PRODUCT	WEIGHT PERCENT YIELD	MOLE PERCENT YIELD FROM N	MOLE PERCENT YIELD FROM C
N_2	9	24		N_2	8	21	
NO	26	32		NO	34	42	
N_2O	23	19		N_2O	13	22	
NH_3	0	0		NH_3	0	0	
HCN	3	4	8	HCN	8	11	22
CO	9		24	CO	12		32
CO_2	15		25	CO_2	13		22
CH_2O	2		5	CH_2O	0		0
CH_4	<1		<5	CH_4	<1		<5
H_2	<1			H_2	<1		
H_2O	12			H_2O	11		
	100	95	65		99	96	76

*SAMPLE 96 PYROLYZED

53

HMX STRUCTURAL MODIFICATION STUDIES

SYNTHESIS OF HMX DERIVATIVES

1-Azidomethyl-3,5,7-Trinitro-1,3,5,7-Tetrazacyclooctane (AZMTTC)

When DPT, a compound readily prepared by nitrolysis of hexamethylenetetramine (Ref. 15), is treated with an equivalent of 98% nitric acid in excess acetic anhydride, 1-acetoxymethyl-3,5,7-trinitro-1,3,5,7-tetrazacyclooctane (AMTTC) is formed (Ref. 16) in 70 to 80% yield (Fig. 2).

Bell and Dunstan (Ref. 17) have investigated reactions of the six-, seven-, and eight-membered ring acetate nitramines with various nucleophiles, such as alcohols and inorganic salts. One aspect of their work was reaction of these ring acetates with sodium azide in efforts to prepare the corresponding ring azide. The reaction of AMTTC and the six-membered ring acetate with sodium azide in dimethylformamide gave primarily decomposition products. Only in the case of the seven-membered ring acetate was it possible to obtain the corresponding azido compound.

Numerous attempts were made in this program at nucleophilic substitution of the acetate group by inorganic azide salts in various solvents and reaction conditions which showed that the eight-membered ring decomposes or that no substitution occurs.

Dunning and Dunning (Ref. 18) have reported that treatment of 1-methoxymethyl-3,5-dinitro-1,3,5-triazacyclohexane with acetyl chloride and acetyl bromide gave the corresponding chloro and bromo derivatives. This chemistry was applied to the eight-membered ring acetate, AMTTC.

Treatment of AMTTC with acetyl bromide gave a near quantitative yield of 1-bromomethyl-3,5,7-trinitro-1,3,5,7-tetrazacylooctane, BrMTTC (Fig. 2). Attempts to convert the bromo derivative to the corresponding azide with sodium azide in various solvents were unsuccessful.
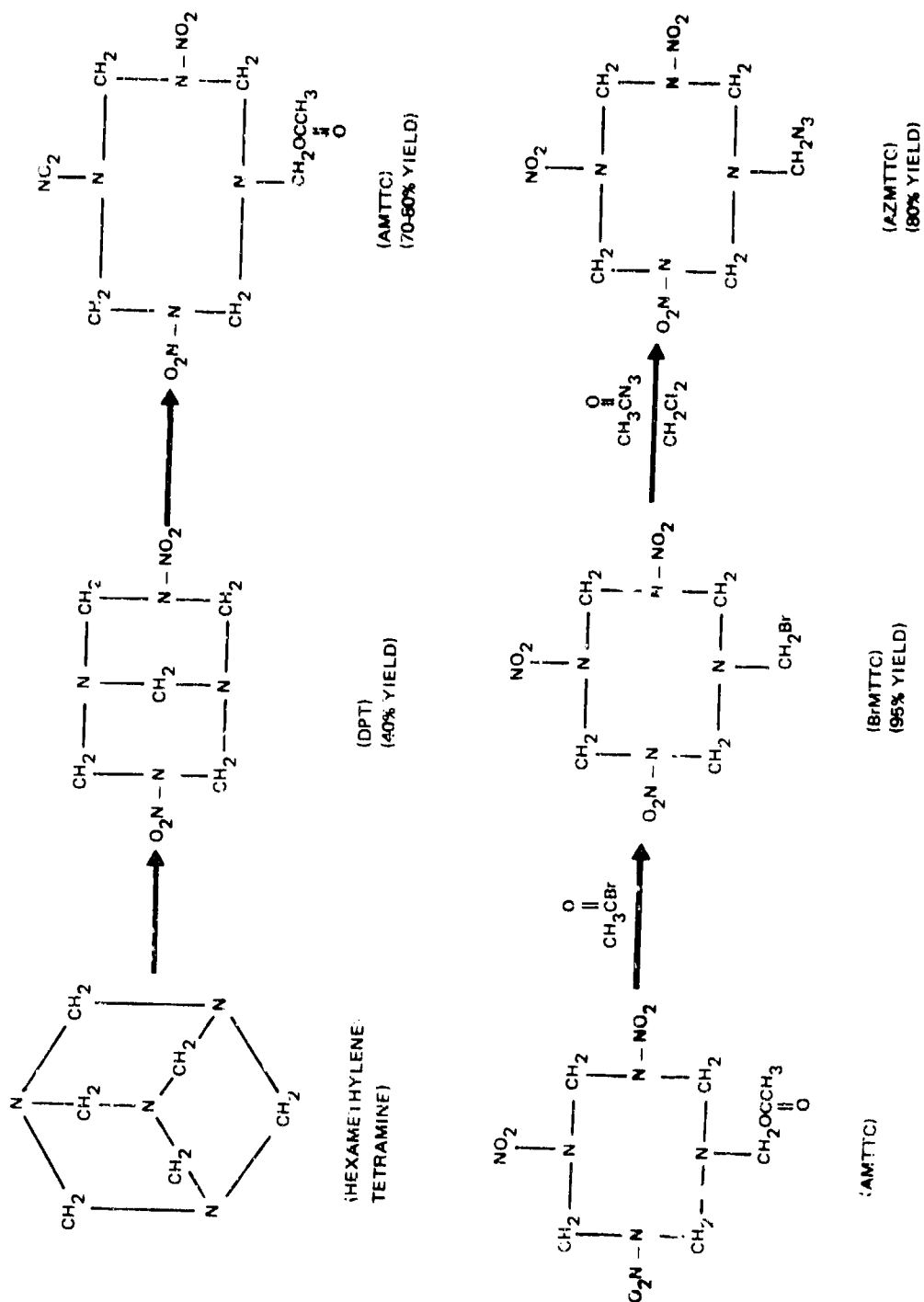
54

Figure 2. Synthesis of 1-Azidomethyl-3,5,7-Trinitro 1,3,5,7-Tetrazacyclooctane (AZMTTC)

55

A novel method then was developed for the conversion of the eight-membered bromo derivative to the corresponding azido compound using acetyl azide as the aziding agent in methylene chloride. The acetyl azide is generated *in situ* in methylene chloride solution at 5 C and is reacted with BrMTTC in a heterogeneous reaction at 10 to 15 C. The low temperature is required since acetyl azide starts to decompose at about 40 C to form methyl isocyanate via the Curtius reaction. The conversion of the bromo derivative to 1-azidomethyl-3,5,7-trinitro-1,3,5,7-tetrazacyclooctane was achieved in 80% yield (Fig. 2).

HPLC analysis gave a single peak and elemental analyses calculated for $C_5H_{10}N_{10}O_6$ are: C, 19.61; H, 3.27; N, 45.75; Found: C, 19.99; H, 3.28; N, 44.99. The compound melts at 130 to 131 C (Ref. 19).

1-Trinitroethyl-3,5,7-Trinitro-1,3,5,7-Tetrazacylooctane (TNTTC)

Nitroform alkylations of aliphatic primary bromo derivatives with silver nitroform have been studied by numerous investigators (Ref. 20). Acetonitrile is a typical solvent used in these studies. Attempts to convert BrMTTC to TNTTC via $AgC(NO_2)_3$ in acetonitrile at ambient temperature were unsuccessful (Fig. 3).

1-(Azidoethoxy) Methyl-3,5,7-Trinitro-1,3,5,7-Tetrazacyclooctane (AEMTTC)

Attempts to convert BrMTTC to AEMTTC via the Williamson synthesis with azidoethanol were unsuccessful (Fig. 3). BrMTTC underwent decomposition under various conditions when azidoethanol was used as the reaction solvent.

1,5-Dinitro-3,7-Dibromoacetyl-1,3,5,7-Tetrazacyclooctane (DNBTTC)

1,5-dinitro-3,7-diacetyl-1,3,5,7-tetrazacylooctane (DADN) was believed to be an attractive structurally symmetrical precursor for attempts to monobrominate both methyl ($-CH_3$) groups to arrive at the precursor DNBTTC (Fig. 4), which then could undergo azide substitution via the novel process developed under
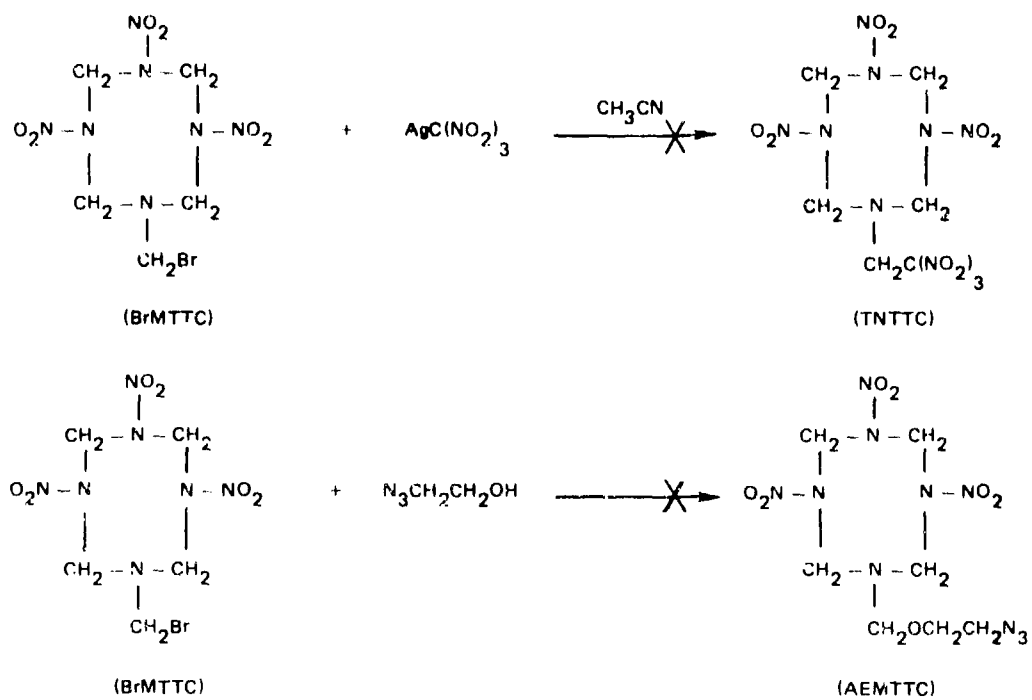
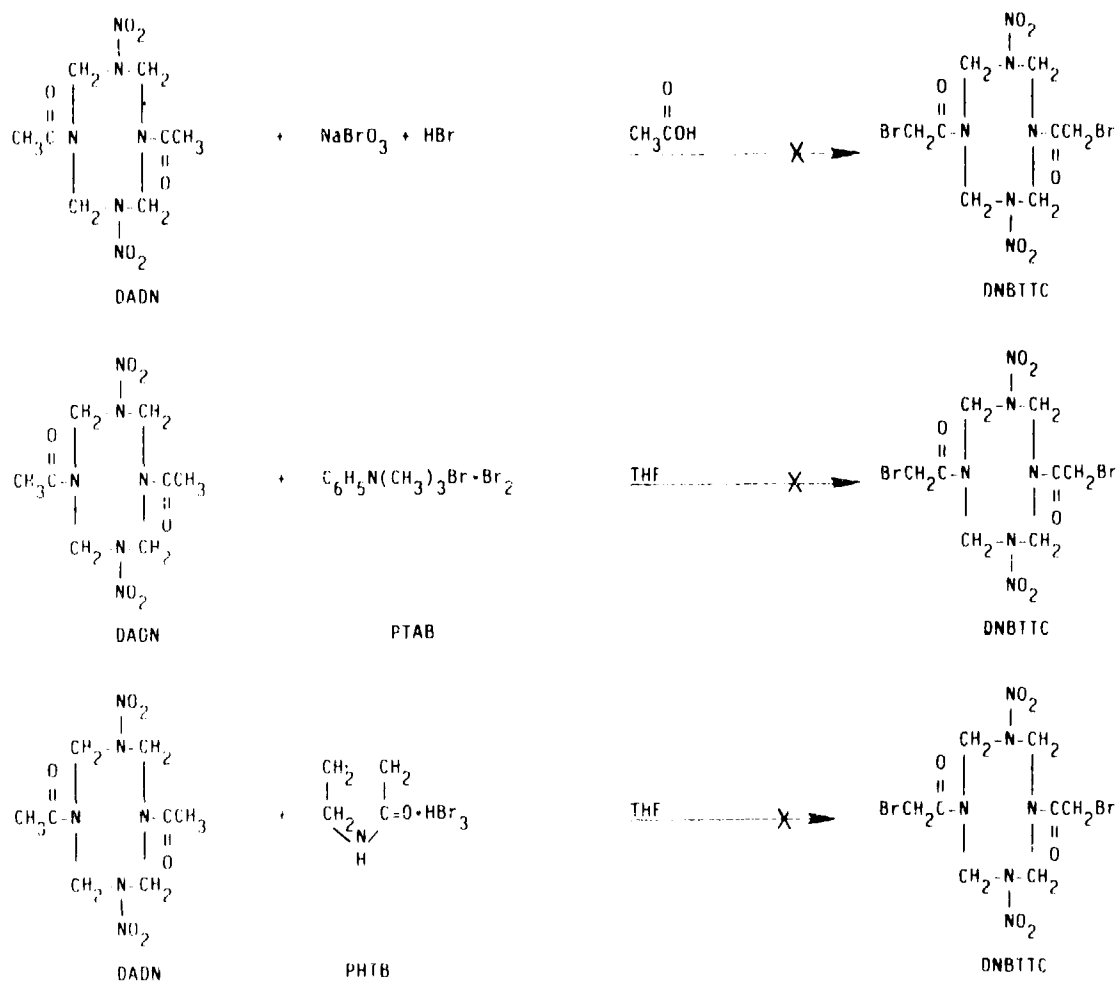Figure 3. Synthesis Attempts of Novel HMX Derivatives

Figure 4. Attempts to Monobrominate Methyl Groups of DADN

this program using acetyl azide in the synthesis of AZMTTC (Fig. 2). However, all attempts made to monobrominate the methyl groups of DADN (Fig. 4) were unsuccessful. The initial attempts utilized a brominating medium consisting of sodium bromate ($NaBrO_3$), aqueous hydrobromic acid (47% HBr), and acetic acid as the reaction solvent (Ref. 21). The reaction parameters investigated were reaction temperature, time, and reactant molar ratios. The only results obtained were recovery of starting material or decomposition-type reactions.

Another approach investigated, based on the literature, involved the use of phenyltrimethylammonium perbromide (PTAB) in tetrahydrofuran (THF) solvent. This reaction system had been successfully used previously for monobrominating a methyl group next to a naphthalene carbonyl ($-C=O$) group (Ref. 22). The reaction parameters investigated in the attempted monobromination of DADN with PTAB were reaction temperature, time, and reactant molar ratios (Fig. 4). In all cases, no reaction occurred.

A final attempt at monobrominating the methyl groups of DADN involved the use of pyrolidone hydrotribromide (PHTB), which was based on a literature preparative method involving a selective brominating agent for ketones (Ref. 23). No reaction between DADN and PHTB occurred under any of the reaction conditions investigated.

1-Aminoethyl-3,5,7-Trinitro-1,3,5,7-Tetrazacyclooctane (AMMTTC)

The successful synthesis of AMMTTC would give an attractive precursor for a number of condensation reactions with activated alcohols followed by nitration to give symmetrical and unsymmetrical HMX derivatives. The initial attempts made to synthesize AMMTTC from the novel precursor 1-bromomethyl-3,5,7-trinitro-1,3,5,7-tetrazacyclooctane (BrMTTC) resulted in the isolation of a compound with elemental analyses far from that theoretically expected (Fig. 5). The reaction of BrMTTC in ammonia-ethanol solutions was further investigated with emphasis on varying reaction temperature and time. In all cases, the eight-membered BrMTTC ring underwent cleavage giving a solid unwanted side product.
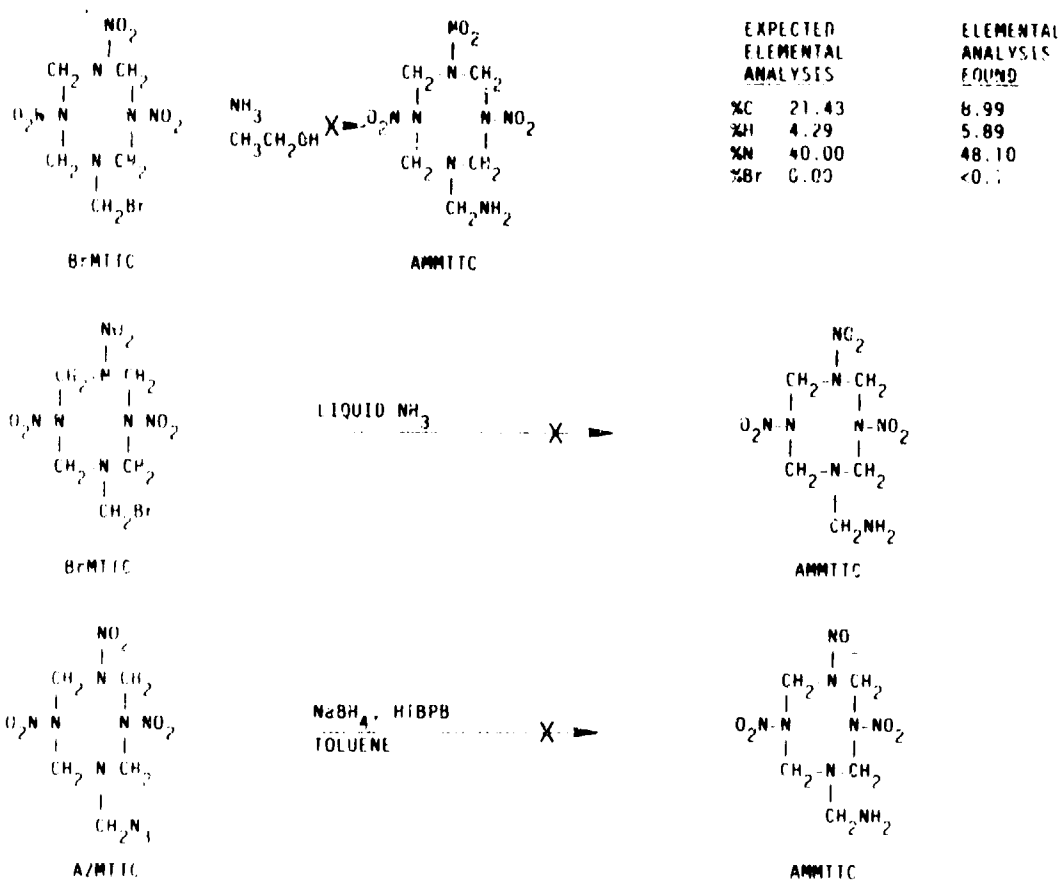
EXPECTED ELEMENTAL ANALYSIS		ELEMENTAL ANALYSIS FOUND
%C	21.43	8.99
%H	4.29	5.89
%N	40.00	48.10
%Br	0.00	<0.1

Figure 5. Attempts to Synthesize 1-Aminomethyl-3,5,7-Trinitro-
1,3,5,7-Tetrazacyclooctane (AMMTTC)

A second approach investigated the reaction of BrMTTC in liquid ammonia at -30 and -40 C at various reaction times (Fig. 5). In all cases, decomposition products were obtained.

A final approach investigated the reduction of the azido group to amine via sodium borohydride ($NaBH_4$) in the presence of a phase transfer catalyst, hexydecyltributylphosphonium bromide (HTBPB), and toluene solvent (Ref. 24). The reaction at ambient temperature resulted in recovery of the starting material without any indication of azide reduction to amine (Fig. 5).

1-Iodomethyl-3,5,7-Trinitro-1,3,5,7-Tetrazacyclooctane (IMNTC)

Synthesis of the novel precursor IMTTC was attempted via the approach used in the synthesis of BrMTTC by reacting 1-acetoxymethyl-3,5,7-trinitro-1,3,5,7-tetrazacyclooctane (AMTTC) with an excess of acetyl iodide (Fig. 6). It was believed that the iodo group would undergo a nucleophillic substitution reaction more readily than BrMTTC under the mild conditions needed to maintain ring integrity (Fig. 3). The reaction of AMTTC with an excess of acetyl iodide for 1 hour at 0 to 5 C gave a light yellow solid with the elemental analyses shown in Fig. 6. These analyses implied approximately 90% iodo substitution, thus indicating a longer reaction time was needed to obtain a quantitative conversion.

PYROLYSIS OF HMX-RELATED COMPOUNDS

Pyrolysis decomposition studies of AZMTTC, as described below, indicated that structural symmetry of HMX derivatives must be maintained to achieve high melting or liquefaction temperatures and a mode of decomposition that would result in comparable rates of C-N and $N-NO_2$ bond cleavage giving increased energy release and generation of reactive gas-phase species. Thus, the studies described above were conducted to provide compounds for further proof of this hypothesis. However, because of the difficulties encountered during the attempted preparations of these candidate compounds, DADN was the only compound investigated other than AZMTTC.

AMTTC
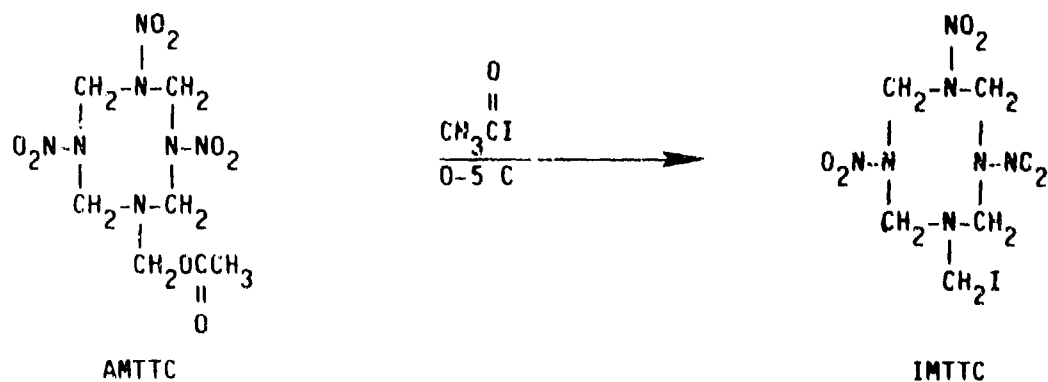
IMTTC

	EXPECTED ELEMENTAL ANALYSIS	ELEMENTAL ANALYSIS FOUND
C	15.34	16.04
H	2.56	2.89
N	25.06	23.23
I	32.48	28.58

Figure 6. Attempted Synthesis of 1-Iodomethyl-3,5,7-Trinitro-
1,3,5,7-Tetrazacyclooctane (IMTTC)

Pyrolysis of DADN

DADN has a melting point of 265 C and is synthesized in a one-pot operation (Ref. 25). The high melting point is one example of the effect of structural symmetry upon HMX derivatives. In addition, high heating rate decomposition studies of DADN demonstrated that the compound decomposed similarly to HMX with respect to covalent C-N and $N-NO_2$ bond cleavage. Table 42 summarizes the gas-phase product distributions of HMX, AZMTTC, and DADN after pyrolysis at 800 C under experimental conditions given in the Experimental Details section.

The gas phase product distribution of DADN (Table 42) implies both C-N (N_2O yield) and $N-NO_2$ (NO yield) bond cleavage are occurring, although a measurable cooling effect is present (higner N_2O yield) probably due to the non-energetic acetyl groups in place of nitro groups. In addition, the cooling effect was indicated from DADN undergoing only 70% pyrolysis.

Pyrolysis of AZMTTC

Pyrolysis decomposition data for AZMTTC showed that covalent C-N bond cleavage was the predominant bond-breaking process occurring during AZMTTC decomposition with very little $N-NO_2$ cleavage occurring. This resulted in high N_2O and CH_2O yields and was found not to be conducive to increased burn rates. During the decomposition of HMX at 800 C it was shown that both $N-NO_2$ (high NO yields) and C-N (N_2O yields) bond cleavage occurred in a competitive manner, which resulted in the product distribution shown in Table 42. In the low-temperature (~300 C) decomposition of HMX (Table 3), C-N bond cleavage was the predominant process resulting in high N_2O and CH_2O yields. It could be concluded then that eight-membered ring tetranitramine compounds that gave high N_2O and/or CH_2O yields after pyrolysis at 800 C would be undergoing predominant C-N bond cleavage with little competing $N-NO_2$ cleavage as found with AZMTTC. It is believed that the lack of structural symmetry is the source of this decomposition mechanism.

TABLE 42. GAS-PHASE PRODUCT DISTRIBUTION FROM PYROLYSIS AT ~800 C, 10 SECONDS, 2 ATM HELIUM

	HMX				AZTEC				DADN*		
PRODUCT	WEIGHT PERCENT YIELD	MOLE PERCENT YIELD FROM N	MOLE PERCENT YIELD FROM C	PRODUCT	WEIGHT PERCENT YIELD	MOLE PERCENT YIELD FROM N	MOLE PERCENT YIELD FROM C	PRODUCT	WEIGHT PERCENT YIELD	MOLE PERCENT YIELD FROM N	MOLE PERCENT YIELD FROM C
N_2	10	26		N_2	10	22		N_2	11	11	
NO	30	37		NO	2	2		NO	19	31	
N_2O	11	13		N_2O	53	74		N_2O	33	72	
NH_3	0	0		NH_3	0	0		NH_3	0	0	
HCN	13	18	16	HCN	0	0	0	HCN	4	7	5
CO	12		32	CO	8		18	CO	1		9
CO_2	11		18	CO_2	5		7	CO_2	24		20
CH_2O	0		0	CH_2O	15		31	CH_2O	0		0
CH_4	<1		<5	CH_4	<1		<4	CH_4	<1		<2
								$CH_2=CH_2$	1		3
H_2	<1			H_2	1			H_2	<1		
H_2O	12			H_2O	6			H_2O	<1		
	99	99	86		100	98	60		99	123	37

*SAMPLE ONLY 70% PYROLYZED

HMX structure:

```
           NO2
            |
      CH2  N-CH2
       |        |
 O2N-N           N-NO2
       |        |
      CH2-N-CH2
            |
           NO2
```

AZTEC structure:

```
           NO2
            |
      CH2-N-CH2
       |        |
 O2N-N           N-NO2
       |        |
      CH2-N-CH2
            |
          CH2N3
```

DADN* structure:

```
           NO2
            |
      O  CH2-N-CH2
      ||   |        |
  CH3-C-N           N-CCH3
       |        |    ||
      CH2-N-CH2      O
            |
           NO2
```

LIQUEFACTION TEMPERATURE	280 C	130 C	265 C

64

SECTION 5

COMBUSTION RATE STUDIES

HMX-BASED SYSTEMS

The effects of selected combustion modifiers were studied in two types of polymer systems: (1) hydroxy-terminated polyester (R-18) plasticized with TMETN, NG, TA, and TVOPA, and (2) hydroxy-terminated glycidyl azide polymer (GAP) containing no plasticizer. The burning rate data are summarized in Table 43 and the symbol (θ) will be used to denote the burning rate at any pressure with the modifiers present to the baseline burning rate.

Triaminoguanidine (TAG) Modifiers

Four compounds containing TAG were examined for burning rate modification: TAGZT, TAGN, TAG·5AT, and TAGNAT. The most extensive series of experiments were carried out with the TAGZT and the following matrix of ingredient combinations were studied:

Oxidizer blends
- 50/50: Class A/Class E
- All Class A

Plasticizer/Polymer = 2:1 and 1:1

Modifier Particle Sizes: 7μ and 50μ

Modifier Levels: 15 to 52.5 weight percent

The utilization of the 50/50 oxidizer blend was maintained as the initial baseline. The augmentation levels for the 30% TAGZT (7μ) system is given in Fig. 7 and the effect of both TAGZT level and particle size in a R-18/TMETN (1:1) system is illustrated in Fig. 8. The relative augmentation factors at constant TAGZT level are similar for TA (1:1), TMETN (1:1), and NG (2:1). However, the TMETN (2:1) system gave a slightly reduced augmentation level.

TABLE 43. BURN RATE DATA SUMMARY

| NITRAMINE TYPE	WEIGHT PERCENT					BURN RATE, CM/SEC, AT AT PRESSURE, MPa				THEORETICAL FLAME TEMPERATURE AT 6.89 MPa, K
	CLASS A	CLASS B	R 18/HMDI	PLASTICIZER	OTHER	1.72	3.45	6.89	10.34	
HMX	37.5	37.5	12.5	12.5 TMETN	-	0.157	0.239	0.462	0.699	2496
	30.0	30.0	12.5	12.5 TMETN	15.0 TAGZT (7u)	0.277	0.452	0.678	0.851	2126
	22.5	22.5	12.5	12.5 TMETN	30.0 TAGZT (7u)	0.495	0.769	1.194	1.519	1777
	22.5	22.5	12.5	12.5 TMETN	30.0 TAGZT (50u)	0.457	0.597	0.940	1.168	1777
	11.2	11.3	12.5	12.5 TMETN	52.5 TAGZT (50u)	0.559	0.765	1.067	1.376	1580
	37.5	37.5	8.7	16.3 TMETN	-	0.196	0.297	0.584	0.775	2743
	22.5	22.5	8.7	16.3 TMETN	30.0 TAGZT (7u)	0.495	0.802	1.171	1.455	2020
	37.5	37.5	12.5	12.5 TA	-	0.091	0.145	0.252	0.340	1805
	22.5	22.5	12.5	12.5 TA	30.0 TAGZT (7u)	0.292	0.490	0.660	0.826	1434
	37.5	37.5	8.3	16.7 NG	-	0.196	0.340	0.597	0.664	2957
	22.5	22.5	8.3	16.7 NG	30.0 TAGZT (7u)	0.673	1.092	1.468	1.562	2238
	37.5	37.5	8.3	16.7 TVOPA	-	0.193	0.315	0.572	0.856	2754
	22.5	22.5	8.3	16.7 TVOPA	30.0 TAGZT (7u)	0.955	1.783	2.149	2.433	2081
	75.0		12.5	12.5 TMETN		*	0.178	0.394	0.594	2496
	45.0	-	12.5	12.5 TMETN	30.0 TAGZT (7u)	0.320	0.579	1.148	1.422	1777
	22.5	22.5	12.5	12.5 TMETN	30.0 TAG-5AT (7u)	0.198	0.373	0.521	0.601	1601
	60.0		12.5	12.5 TMETN	15.0 TAGN (4u)	0.216	0.368	0.665	0.965	2288
	22.5	22.5	12.5	12.5 TMETN	30.0 TAGN (50u)	0.175	0.315	0.572	0.838	2095
			12.5	12.5 TMETN	75.0 TAGN (50u)	0.279	0.419	0.711	0.884	1570
	28.1	28.1	12.5	12.5 TMETN	18.8 DATH (13u)	0.183	0.292	0.521	0.749	2465
	22.5	22.5	12.5	12.5 TMETN	30.0 DATH (13u)	0.236	0.404	0.721	0.978	2448
	-	-	12.5	12.5 TMETN	75.0 DATH (13u)	0.386	0.813	1.453	2.007	2382
	25.0	25.0	12.5	12.5 TMETN	25.0 AZMTTC (20u)	0.140	0.315	0.495	0.742	2309
	22.5	22.5	12.5	12.5 TMETN	30.0 AP (30u)	0.495	0.600	0.790	0.961	2812
	10.0		12.5	12.5 TMETN	5.0 AP (1u)	0.157	0.411	0.754	1.143	2546
	22.5	22.5	12.5	12.5 TMETN	30.0 DAZT (25u)	*	*	0.584	1.374	1756
	22.5	22.5	12.5	12.5 TMETN	30.0 ANAT (25u)	0.244	0.444	0.686	0.919	2044
	22.5	22.5	12.5	12.5 TMETN	30.0 TAGNAT (20u)	0.254	0.376	0.653	0.884	1968
	22.5	22.5	12.5	12.5 TMETN	30.0 HN (40u)	0.208	0.452	0.704	0.940	2421
	21.5	21.5	12.5	12.5 TMETN	20.0 TMAAZ (30u)	0.147	0.249	0.411	0.572	1619
	30.0	30.0	12.5	12.5 TMETN	15.0 ABMF (15u)	0.191	0.343	0.572	0.772	2449
	30.0	30.0	12.5	12.5 TMETN	15.0 AMDTH (33u)	0.140	0.259	0.444	0.597	2339
	36.0	36.0	12.5	12.5 TMETN	3.0 LIN$_3$ (12u)	0.173	0.340	0.564	0.754	2413
	37.5	37.5	8.3	12.7 TSMTN	4.0 CMP (LIQUID)	0.168	0.292	0.574	0.899	2559
RDX	37.5	37.5	12.5	12.5 TMETN		0.119	0.221	0.432	0.630	2502
	30.0	30.0	12.5	12.5 TMETN	15.0 TAGZT (7u)	0.266	0.460	0.667	0.911	2134
	22.5	22.5	12.5	12.5 TMETN	30.0 TAGZT (7u)	0.678	0.886	1.214	1.478	1781
	37.5	37.5	8.3	16.7 NG		0.112	0.280	0.629	0.965	2964
	22.5	22.5	8.3	16.7 NG	30.0 TAGZT (7u)	0.693	1.139	1.557	1.963	2243
	60.0		12.5	12.5 TMETN	15.0 TAGN (4u)	0.203	0.348	0.518	0.732	2295
	22.5	22.5	12.5	12.5 TMETN	30.0 TAG-5AT (7u)	0.264	0.419	0.622	0.787	1605
	35.0	35.0	12.5	12.5 TMETN	5.0 CU WS	0.211	0.309	0.556	0.886	2436
	22.5	22.5	12.5	12.5 TMETN	30.0 DATH (13u)	0.206	0.381	0.648	0.889	2452
	75.0		12.5	12.5 TMETN		0.111	0.186	0.362	0.559	2502

*DID NOT BURN
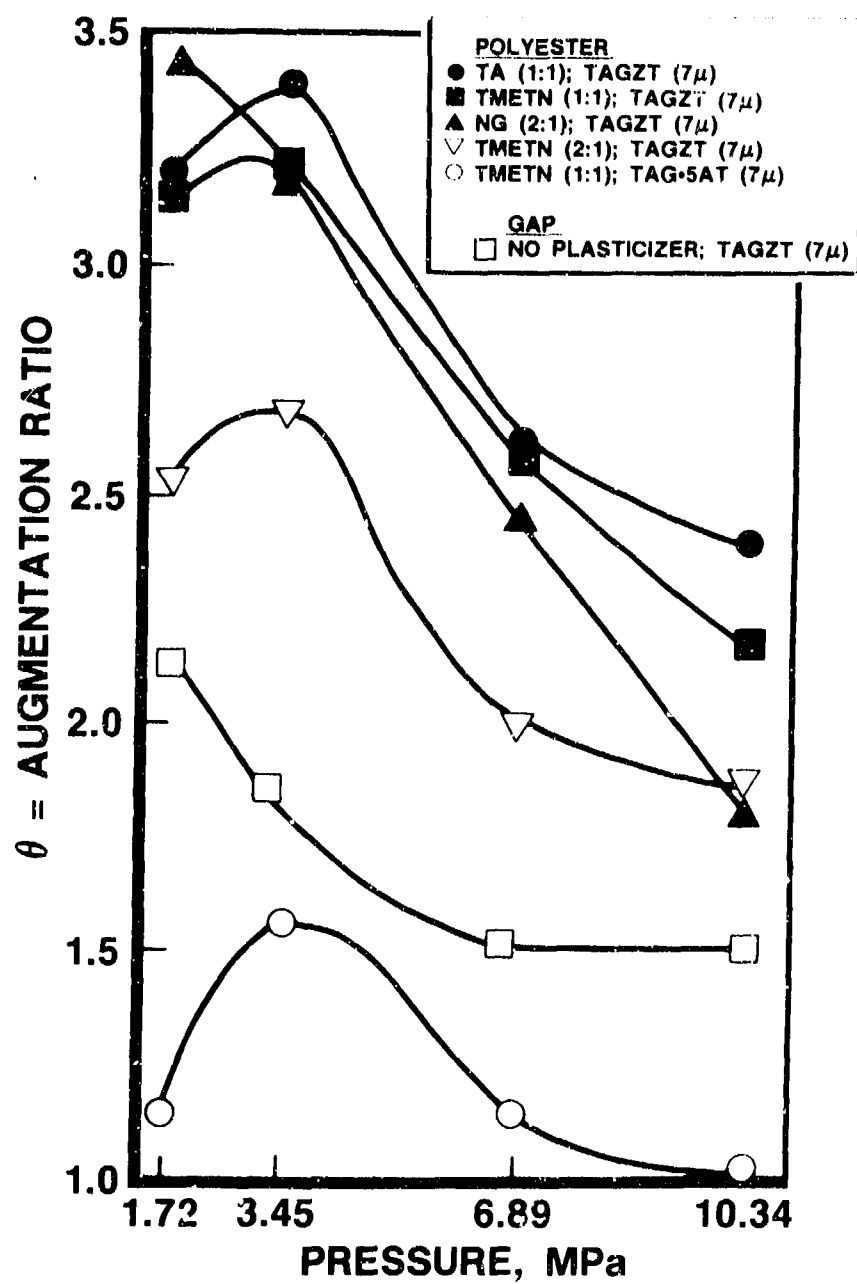
Figure 7. Burn Rate Augmentation with 30% TAG-Type
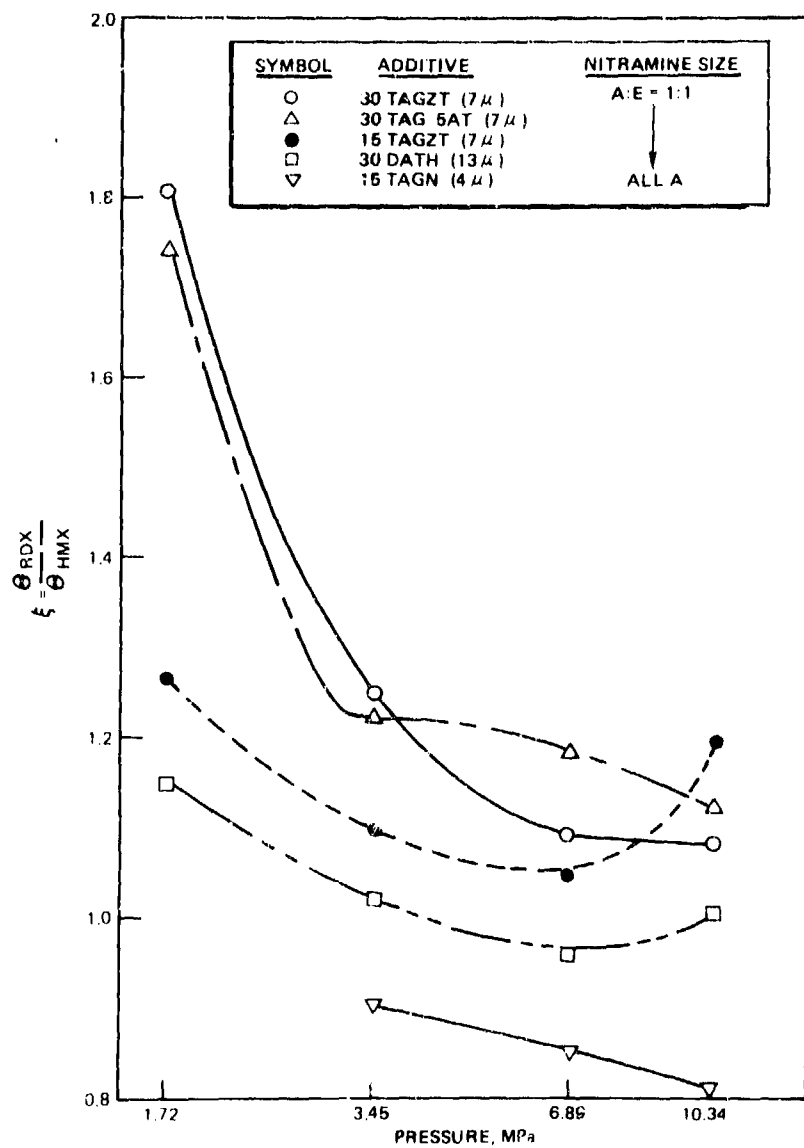Additives [HMX(A)/(E)=1:1]

Figure 8. Relative Augmentation of RDX/HMX

68

Fine TAGZT (7μ) is more effective than coarse TAGZT (50μ), which suggests that diffusional effects and the rate of NH_3 production are of primary importance. Increasing the concentration of TAGZT increased the augmentation level, which is in accordance with the concept of accelerated rate via the reaction of amidogen (NH_2) radicals reacting with the NO produced from the HMX decomposition.

The correlation of burning rate at 6.89 MPa for the pure HMX and 30% TAGZT systems is shown in Fig. 9. The burning rate can be expressed in the form:

$$r = A\exp\left(-E/RT_f\right)$$
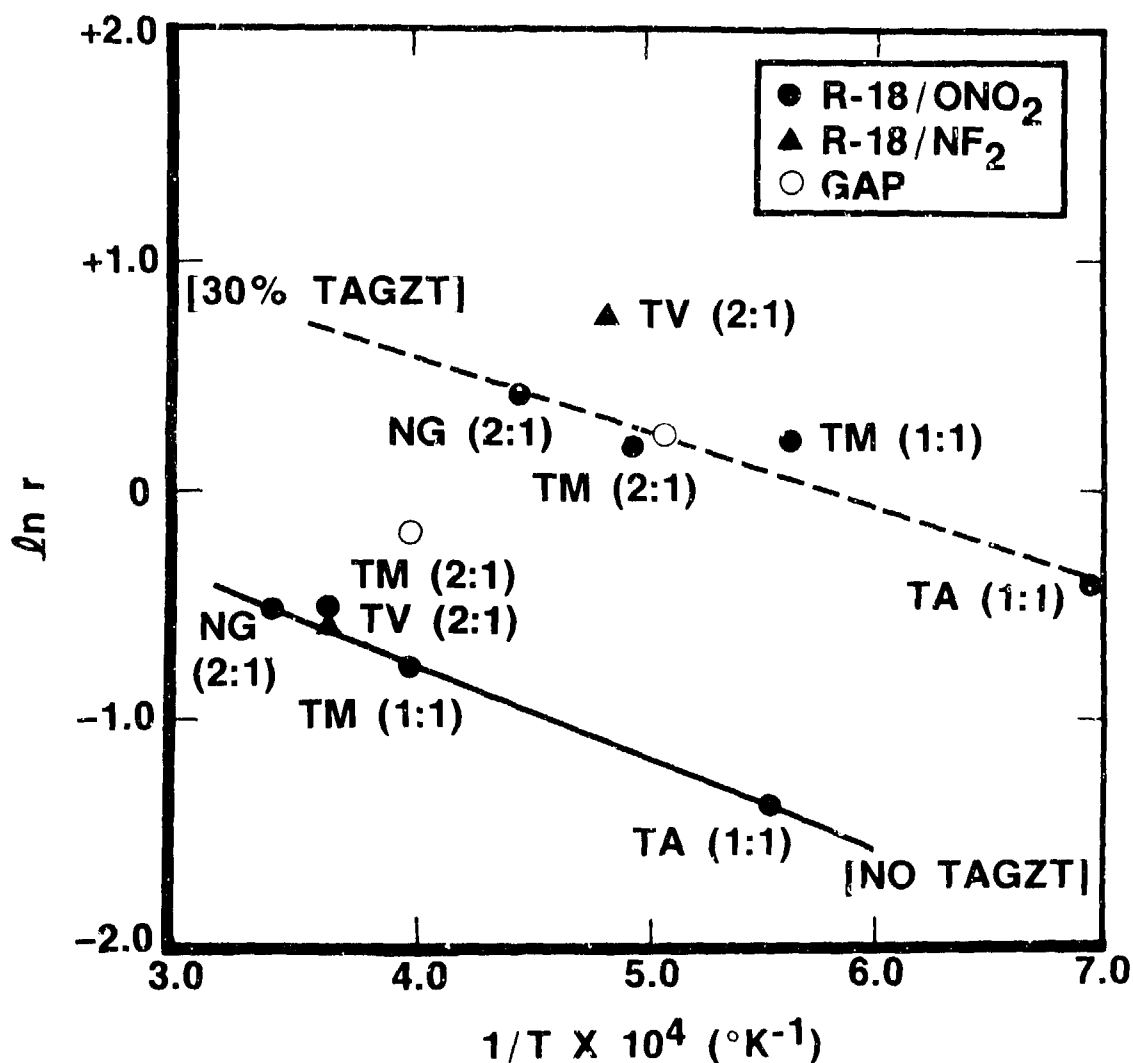
Figure 9. Burn Rate Correlation for Pure HMX
and TAGZT Substituted Systems

69

The two curves in Fig. 9 have very similar slopes and all the plasticizer in the inert R-18 binder fall on the curves with the exception of the difluoroamino ($-NF_2$) plasticizer TVOPA. Propellants containing TVOPA were prepared to "check" the postulated augmentation mechanism:

$$NO + NH_2 \cdot \rightarrow N_2 + H_2O + Q_1$$
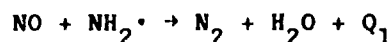
This equation is a global summary of the key steps in a very complex reaction. The incorporation of TVOPA will result in the formation of $NF_2 \cdot$ radicals, which then can interact with the amidogen radical via the equation:

$$NF_2 \cdot + NH_2 \cdot \rightarrow N_2 + 2HF + Q_2$$
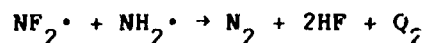
Again, this is a global summary of several reactions. However, it is expected that the NF_2-radical will react more rapidly with NO than the NH_2-radical. No data could be found on this reaction, but the kinetics of $NF_2 \cdot$ reactions with other materials, such as H_2 and C_xH_y compounds, is known to be considerably faster than the comparable NO reaction.

The NG- and TVOPA-based propellants with no TAGZT present have virtually the same burning rate. However, the 30% TAGZT system containing TVOPA burns considerably faster than the NG analog.

Although the heat release from the NO system (Q_1) is 60 kcal lower than the heat release (Q_2) from the NF_2 system, the actual concentrations of reactive species is virtually the same. Only 1.2% additional heat can be generated based upon the stoichiometric equations. In fact, the overall theoretical flame temperature of the TVOPA system is 91% of the NG system (due to other overall product distributions).

The stoichiometry is based upon the percent of NO generated from the HMX decomposition experiments and the percent of NH_3 generated from the TAGZT decomposition experiments. This is coupled to an assumed NO production level from NG decomposition and NF_2 production level from TVOPA decomposition.

70

Both plasticizers contribute very little in terms of reactive species (concentration wise). The main point to be made is that the $(NF_2\cdot + NH_2\cdot)$ reaction is kinetically faster and initiates a further series of reactions which lead to the higher burning rates. In effect, TVOPA could be considered as a "pseudocatalyst."

Utilization of TAG·5AT resulted in considerably lower augmentation ratios than the TAGZT systems. This phenomena is believed to be related to the decomposition mode previously discussed in the Decomposition Experiments section.

Both TAGN and TAGNAT yielded augmentation rates lower than TAGZT and both materials contain oxygen. The presence of oxygen reduces the amount of NH_3 formed for diffusional interaction. However, other investigations and past experience with TAGN suggest that a "mismatching" of TAGN and HMX particle sizes may be a very critical factor. A 70% augmentation was obtained at the 15% TAGN (4μ) level when only Class A-HMX was employed. Additional experiments would be required to explain this apparently very complex mechanism.

Ammonium and Hydrazine Modifiers

The ammonium salt analogs of TAGZT(DAZT) and TAGNAT(ANAT) were investigated at the 30% addition level. The DAZT system yielded a 26% increase in the burning rate, while the ANAT exhibited a 48% improvement.

The DAZT system is very puzzling in its behavior. Combustion could not be sustained below 5.2 MPa and an exponent greater than 2 was observed above this pressure. Reasonable levels of NH_3 were observed in the decomposition experiments, but a large quantity of N_2H_4 (26%) also was observed. The N_2H_4 persisted in the decomposition experiments when the mixed HMX-DAZT system was studied. This suggests that N_2H_4 is not as desirable as NH_3 for rate acceleration. One propellant containing 30% hydrazine nitrate (HN) showed a 52% increase in rate, which slightly confuses the issue. However, the HN was not nearly as effective as TAGZT.

71

The increase in burning rate observed for the ANAT system may be more a result of the fast burning rate of pure ANAT (Ref. 26). The decomposition experiments indicated that no NH_3 was produced and a trace amount of N_2H_4 was formed.

Finally, two propellants containing AP were examined. Substitution of 30% AP (30μ) augmented the rate by 71% at 6.89 MPa, and substitution of 5% AP (1μ) augmented the rate by 63% at 6.89 MPa. AP produced both NH_3 and $HClO_4$ upon decomposition and the high level of augmentation for such a small quantity of material again suggests an extremely complex mechanism.

Azido Modifiers

Five compounds containing azido groups were investigated as potential modifiers: (1) AMDTH, a cyclic azido nitramine with adjacent methyl groups in the ring, (2) AZMTTC, the azido-substituted HMX, (3) DATH, a linear diazido nitramine, (4) TMAAZ, a azido tetramethyl ammonium salt, and (5) lithium azide.

In general, the azido compounds were not effective in augmenting the burn rate. However, the linear azido nitramine DATH is known to be a fast-burning ingredient by itself. The previous discussion has indicated some insight into the reasons for this behavior. The propellant in which DATH completely replaced HMX exhibited a 214% increase in rate. However, substitution of only 30% DATH resulted in only a 56% improvement in rate, which indicates little, if any, decomposition product interaction. This correlates with the decomposition studies discussed in the Pyrolysis of HMX-DATH Mixture section.

The propellant containing 18.8% "coprecipitated" DATH yielded a 13% increase in burn rate. The DATH and HMX were in more intimate contact in this experiment but this appears to have had little effect on the rate. Therefore, it is concluded that the DATH increases the rate primarily by an "additive" method rather than an interaction mechanism.

72

Azido (GAP) System

Pure glycidyl azide polymer (GAP) has a unique high-burning rate. Therefore, a series of experiments were carried out to compare the effects of TAGZT on HMX in GAP systems. The data are summarized in Table 44 and illustrated in Fig. 10.

On Contract FO4611-82-C-0043 with AFRPL, the type of isocyanate has been found to profoundly change the burning rate of GAP gumstocks, which lead to carrying out each experiment with both HMDI and N-100 curing agents. Incorporation of 35 and 75% (50:50 Class A/E-HMX) reduced the burning rate of the GAP systems. Figure 10 illustrates the data only for the HMDI system but, suprisingly, virtually no difference in burning rate is observed with HMX content. The incorporation of 30% TAGZT (7µ) augmented the rate at 6.89 MPa by 50%, which is considerably lower than any of the R-18-based system. The absolute burning rate is comparable to the R-18 systems despite the implicit higher rate of GAP itself. Figures 9 and 10 show the comparative effects of R-18 and GAP-type systems, respectively.

TABLE 44. BURNING RATE OF GAP BASED SYSTEMS

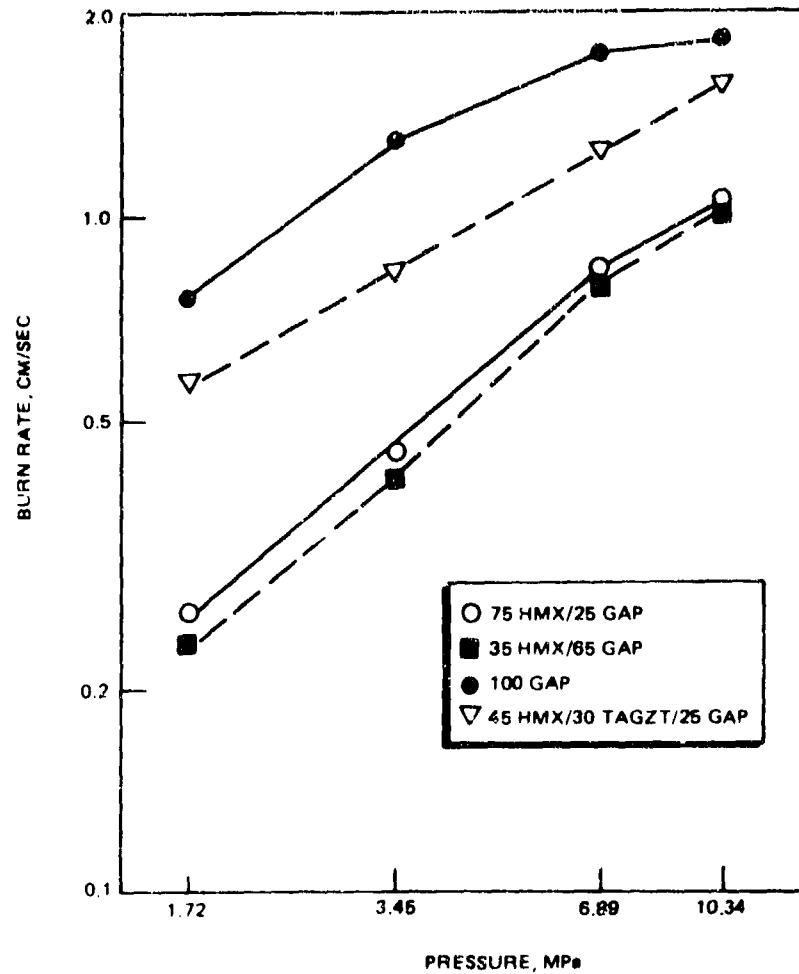| HMX(A)	HMX(E)	WEIGHT PERCENT GAP/NCO TYPE	OTHER	BURN RATE, IN ... AT ... MPa 1.72	3.45	6.89	...	...
37.5	37.5	25.0/HMDI		0.264	0.456	0.8...	.046	
37.5	37.5	25.0/N-100		0.173	0.345	0.4...	0.49...	
17.5	17.5	65.0/N-100		0.177	0.438	0.744	.04	
17.5	17.5	65.0/HMDI		0.231	0.436	0.742...	19	
22.5	22.5	25.0/HMDI	30.0 TAGZT (7µ)	0.574	0.82...	1.25...		
22.5	22.5	25.0/N-100	30.0 TAGZT (7µ)	0.404	0.724			
		100.0/HMDI*		0.762	1.12...			
		100.0/N-100*		0.293	0.447	0.60...		

*DATA OBTAINED ON CONTRACT F-04611-82-C-0043

Figure 10. Burning Rate of GAP Systems (HMDI Curative)

Other Modifiers

Incorporation of 3% LiN_3 increased the burning rate at 6.89 MPa by 22%. A larger increase might have been predicted based on the decomposition experiments, but flame-zone interactions may physically separate the reactive intermediates and larger quantities of LiN_3 would result in several other problems in terms of a practical propellent.

74

The utilization of CMP at the 4% level yielded a small increase in burning rate but nothing comparable to the results obtained in AP-based systems. Fifer and Cole (Ref. 27) found that B-H compounds appear to be effective in accelerating nitramine burning rates, but the current results are not as encouraging.

Reports in Soviet literature (Ref. 28) indicate that the azo (-N=N-)-type nitramines are extremely rapid burning compounds. One propellant containing 15% ABNF yielded an increase of 24% in the rate that was equivalent to the 30% TAGN-substituted system.

RDX-BASED SYSTEMS

A selected number of propellants containing RDX were investigated to obtain comparative data, which is summarized in Table 43.

Triaminoguanidine (TAG) Modifiers

Comparative data was obtained for the three salts TAGZT, TAG·5AT, and TAGN. Figure 11 illustrates that TAGZT is more effective with RDX at low pressure, but similar augmentation rates are obtained with HMX at high pressure (≥ 6.89 MPa). Figure 12 is a comparison of the ratios (ζ) of the augmentation rates of RDX and HMX. In general, most modifiers are more effective with RDX at low pressures. Both TAGZT and TAG·5AT decompose at a temperature more closely matched to RDX than HMX (Structural Modification section), which suggests a closer matching of chemical reaction induction times. Additionally, TAGN should interact more effectively with RDX than HMX for the same reason even though no experimental data were obtained during the current work.

Other Modifiers

The azido-Werner complex $[Cu(NH_3)_2(N_3)_2]$ was investigated at the 5% level and a 29% augmentation was obtained. The compound is extremely difficult to handle (Decomposition Experiments section) and only the one experiment was carried out due to its sensitivity.
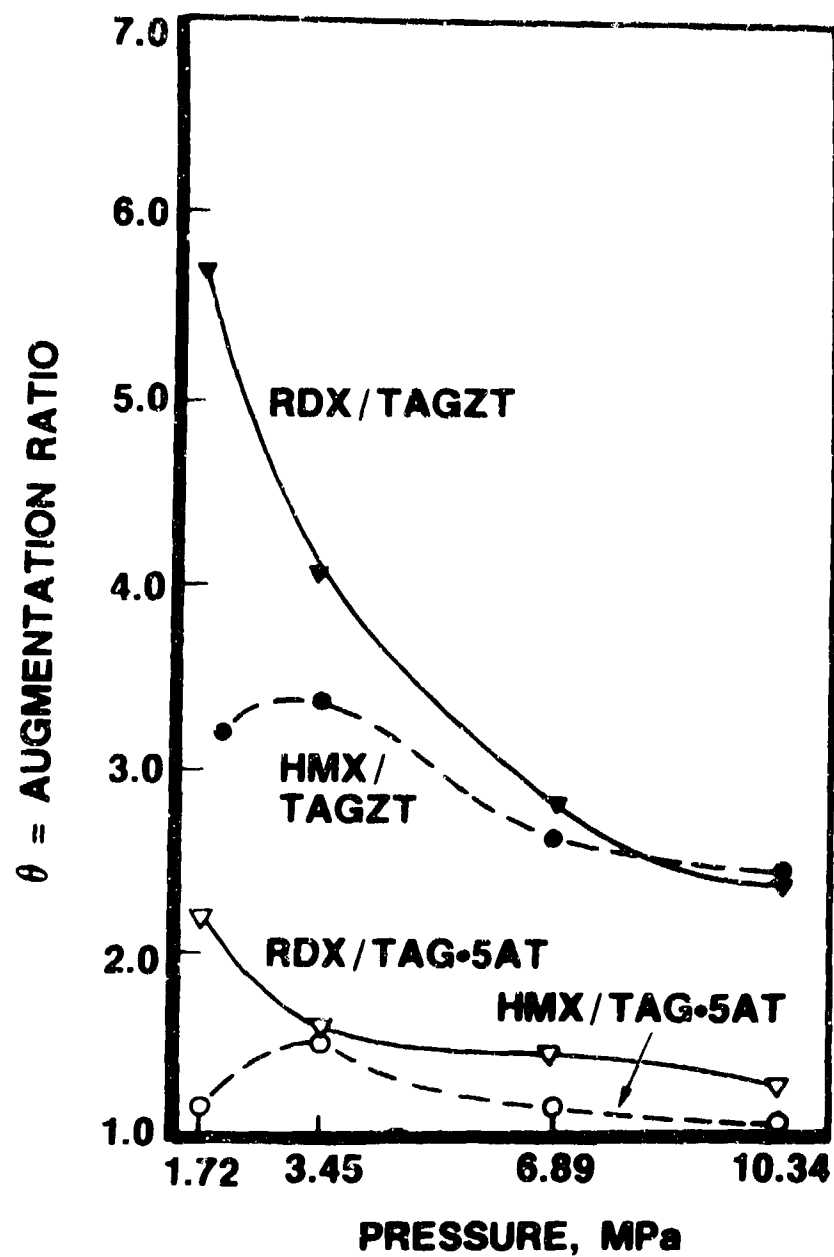
Figure 11.   Comparison of RDX and HMX with 30%
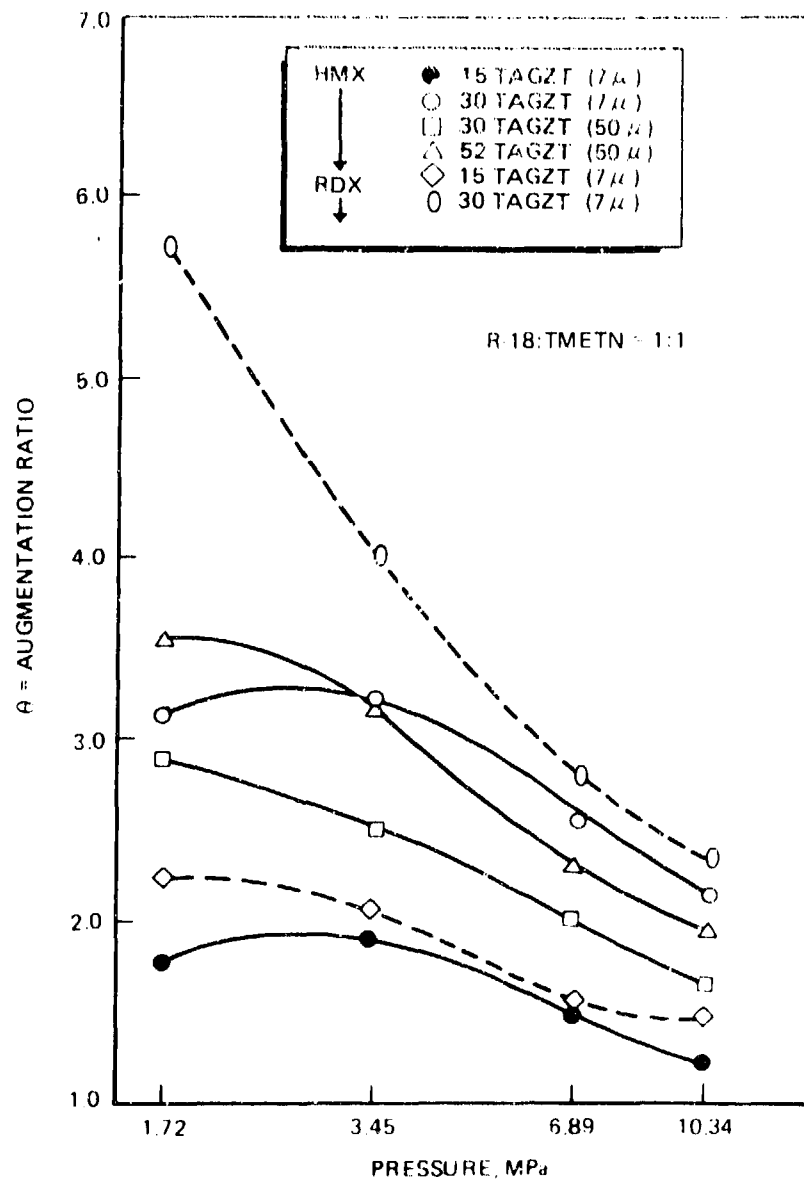   TAG-Type Additives (7µ)

Figure 12.   Effect of TAGZT Concentration and
Particle Size on Burn Rate

77

One experiment was carried out with the diazido linear nitramine (DATH) and augmentation rates similar to HMX were observed.

FLAME ZONE PHENOMENA

The experimental evidence indicates that the incorporation of ammonium generators (especially TAGZT) is the primary factor in achieving good augmentation rates. A physical interpretation of this phenomenon is based on the key reaction (NH_2 + NO $\rightarrow$ N_2 + H_2O), although the actual process is extremely more complicated.

The recent work of Kubota (Ref. 29) has shown that the combustion of HMX-based propellants yields three gas-phase zones and that the reaction of NO may be the limiting step. This experimental evidence lends credence to the concept of accelerated rates via the interaction of amidogen (NH_2) radials with NO.

The generation of NH_2 from NH_3 is an extremely complex process that is highly dependent on the concentration of several other species (Ref. 8, 11, and 29 through 32). It is apparent that the NH_2 + NO reaction is favored in a specific temperature region and is highly concentration dependent. Figure 13 is a schematic representation of the "favored" temperature region.
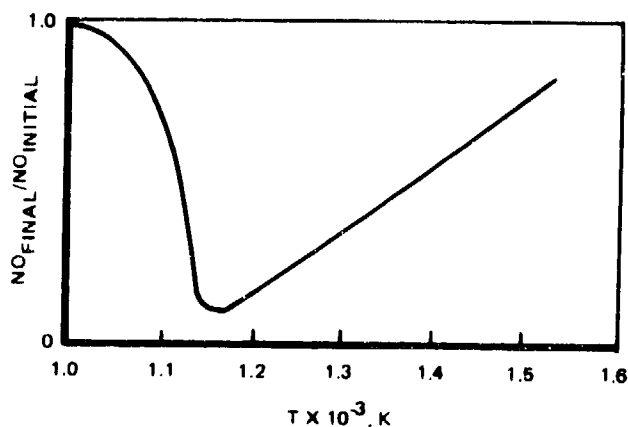

Figure 13.   NO Reaction Parameters

The "mismatching" of HMX/RDX and NH_3-generator particle sizes appears to be the most important factor in accelerating the rate. However, the generation of the proper concentration of NH_3 at the proper temperature might be almost as important. Each NH_3-generating ingredient will yield a different amount of liberated heat and materials such as TAGN are capable of "self-consumption" since they are oxygen-containing materials versus TAGZT and TAG·5AT.

Utilization of very small particles of the TAG salts results in a more complete "encircling" of the nitramine particle, which will result in better diffusional mixing of the reactive gases.

The experiments described in the triaminoguanidine (TAG) modifiers section, which utilized TVOPA (NF_2· generator), play an influential role in "validating" the flame zone concepts with regard to the catalysis via amidogen radicals.

SECTION 6

PRESENTATIONS AND PUBLICATIONS

1. Summaries of the program were presented at the Annual AFOSR Contractors Meetings, March 1982, 1983, and 1984, Lancaster, CA

2. Presentations were given at the 19th and 20th JANNAF Combustion Meetings (Greenbelt, MD, October 1982 and Monterey, CA, October 1983)

3. A presentation was given at the AFRPL Nitramine Workshop, August 1982, Lancaster, CA

4. Frankel, M.B. and D.O. Woolery, <u>J. of Org. Chem.</u>, Vol. 48, Pg. 611 (1983)

REFERENCES

1. Brill, T.B. and R.J. Karpowicz: J. Phys. Chem., 86, 4260 (1982).

2. Goshgarian, B.B., et al.: "Initial Thermochemical Decomposition Mechanisms of Energetic Ingredients: Deuterium Isotope Effects and Isothermal Reaction Studies." Chemical Rocket Research Meeting, Lancaster, CA, 1983.

3. Miles, M.H., et al.: Propellants, Explos. Pyrotech., 7, 100-106, (1982).

4. Axworthy, A.E., et al.: AFATL-TR-80-58, May 1980.

5. CO_2 Laser Radiation Induced Decomposition of Propellant Ingredients, Hercules, Inc., Contract F04611-81-C-0005, July 1981.

6. Shaw, R.A. and F.E. Walker: J. Phys. Chem., 81, 2672 (1977).

7. Cornu, A.J.: Compilation of Mass Spectral Data, Vol. 1, 1975.

8. Miller, J.A., et al.: Comb and Flame, 43, 81 (1981).

9. Baulch, D.L., et al.: Evaluated Kinetic Data for High-Temperature Reactions, Vol. 3, 1976.

10. Kirk, R.E. and D.F. Othmer, Encyclopedia of Chemical Technology, Vol. 9, 1952.

11. Branch, M.C., et al.: Comb. Sci. and Tech., Vol. 29, 147 (1982).

12. Prount, E.G. and V.C. Liddiard: J. Inorg. Nucl. Chem., 35, 2183-2193 (1973).

13. Walker, R.F.: J. Phys. Chem. Solids, 29, 985-1000 (1968).

14. Brill, T.B., et al.: "The Role of Solid-Phase Phenomena in Nitramine Properties and Decomposition," AFOSR/AFRPL Chemical Rocket Research Meeting, March 1983.

15. Bachmann, W., et al.: J. Amer. Chem. Soc., 73, 2769 (1951).

16. Bachmann, W. and E.L. Jenner: J. Amer. Chem. Soc., 73 2773 (1951).

17. Bell, J.A. and I. Dunstan: J. Chem. Soc. (C), 862-869 (1969).

18. Dunning, K.W and W.J. Dunning: J. Chem. Soc., 2925 (1950).

19. Frankel, M.B. and D.O. Woolery: J. Org. Chem., 48, 611 (1983).

20. Hammond, G.S., et al.: Tetrahedron, Vol. 19, Suppl. 1, 177-195 (1963).

21. Wommack, J.B. and D.E. Pearson: J. Chem. Soc., 1307 (1940).

22. Marquet, A. and J. Jacques: Bull. Soc. Chem., France, 90 (1962).

23. Awang, D.V.(and Saul Wolfe: Canadian J. Chem., 47, 706 (1969).

24. Rolla, F.: J. Org. Chem., 47 4327-4329 (1982).

25. Sick, V.I., et al.: Propellants and Explosives," $\underline{6}$, 67-73 (1981).

26. Smith, J.O., et al.: Paper presented at the 1981 JANNAF Propulsion Meeting, New Orleans, LA, May 1981.

27. Fifer, R.A. and J.E. Cole: 16th JANNAF Combustion Meeting, Monterey, CA, Vol. I, 377-398, September 1979.

28. Fogel'zang, A.E., et al.: Fiz. Goren. Vzryva, $\underline{12}$, 827 (1976).

29. Kubota, N.: "Physiochemical Processes of HMX Propellant Combustion," 19th Symposium (International) on Combustion, 777-784, (1982).

30. Anderson, P., et al.: "Direct Investigation of the NH_2+NO Reaction by Laser Photolysis at Different Temperatures," 19th Symposium (International) on Combustion, 11-22, (1982).

31. Dean, A.M., et al.: "Kinetics and Mechanism of NH_3 Oxidation," 19th Symposium (International) on Combustion, 97-105, (1982).

32. Mazio, L.J. and J.K. Arand: "Gas Phase Decomposition of Nitric Oxide in Combustion Products," 16th Symposium (International) on Combustion, 199-208, (1976).

GLOSSARY

ABNF	azobisnitroformamidine
AFRPL	Air Force Rocket Propulsion Laboratory
AEMTTC	1-(azidoethoxy)methyl-3,5,7-trinitro-1,3,5,7-tetrazacyclooctane
AMDTH	1-azidomethyl-3,6-dinitro-1,2,6-triazacycloheptane
AMMTTC	1-aminomethyl-3,5,7-trinitro-1,3,5,7-tetrazacyclooctane
AMTTC	1-acetoxymethyl-3,5,7-trinitro-1,3,5,7-tetrazacyclooctane
ANAT	ammonium 5-nitraminotetrazole
AZMTTC	1-azidomethyl-3,5,7-trinitro-1,3,5,7-tetrazacyclooctane
BRMTTC	1-bromomethyl-3,5,7-trinitro-1,3,5,7-tetrazacyclooctane
CMP	carboranyl-methyl propionate
CUWS	copper ammonium azide Werner complex
DADN	1,5-dinitro-3,7-diacetyl-1,3,5,7-tetrazacyclooctane
DATH	1,7-diazido-2,4,6-trinitrazaheptane
DAZT	diammonium azobitetrazole
DMF	dimethylformamide
DMSO	dimethylsulfoxide
DNATTC	1,5-dinitro-3,7-azidoacetyl-1,3,5,7-tetrazacyclooctane
DNBTTC	1,5-dinitro-3,7-dibromoacetyl-1,3,5,7-tetrazacyclooctane
DPT	1,5-methylene-3,7-dinitro-1,3,5,7-tetrazacyclooctane
DSC	differential scanning calorimetry
GAP	glycidyl azide polymer
HMX	1,3,5,7-tetranitro-1,3,5,7-tetrazacyclooctane
HMDI	hexamethylenediisocyanate
HN	Hydrazine Nitrate
IMTTC	1-iodomethyl-3,5,7-trinitro-1,3,5,7-tetrazacyclooctane
N-100	polyfunctional isocyanate
NG	nitroglycerin
RDX	1,3,5-trinitro-1,3,5-triazacyclohexane
R-18	hydroxy-terminated polyester
TA	triacetin
TAG	triaminoguanidine

TAGN	triaminoguanidinium nitrate
TAG·5AT	triaminoguanidinium-5-aminotetrazole
TAGNAT	bis-triaminoguanidinium 5-nitraminotetrazole
TAGZT	bis-triaminoguanidium azobitetrazole
TMAAZ	tetramethylammonium azide
TMETN	trimethylolethylethane trinitrate
TNTTC	1-trinitroethyl-3,5,7-trinitro-1,3,5,7-tetrazacyclooctane
TVOPA	1,2,3-tris [α,β-bis(difluoramino)ethoxy] propane
w/o	weight percent